Extended ensemble approach to transferable potentials for low resolution coarse-grained models of ionomers

Joseph F. Rudzinski,^{†,¶} Keran Lu,[‡] Scott T. Milner,[‡] Janna K. Maranas,[‡] and William G. Noid*,[†]

†Department of Chemistry, The Pennsylvania State University, University Park,
Pennsylvania 16802

‡Department of Chemical Engineering, The Pennsylvania State University, University

Park, Pennsylvania 16802

¶Current Address: Max Planck Institute for Polymer Research, 55128 Mainz, Germany

E-mail: wnoid@chem.psu.edu

Abstract

We develop an extended ensemble method for constructing transferable, low-resolution coarse-grained (CG) models of polyethylene-oxide (PEO)-based ionomer chains with varying composition at multiple temperatures. In particular, we consider ionomer chains consisting of 4 isophthalate groups, which may be neutral or sulfonated, that are linked by 13 PEO repeat units. The CG models represent each isophthalate group with a single CG site and also explicitly represent the diffusing sodium counterions, but do not explicitly represent the PEO backbone. We define the extended ensemble as a collection of equilibrium ensembles that are obtained from united atom (UA) simulations at 2 different temperatures for 7 chemically distinct ionomers with varying degrees of sulfonation. We employ a global force-matching method to determine the set of interaction potentials that, when appropriately combined, provide an optimal approximation to the many-body potential of mean force for each system in the extended ensemble. This optimized xn force field employs long-ranged Coulomb potentials with system-specific dielectric constants that systematically decrease with increasing sulfonation and temperature. An empirical exponential model reasonably describes the sensitivity of the dielectric to sulfonation, but we find it more challenging to model the temperature-dependence of the dielectrics. Nevertheless, given appropriate dielectric constants, the transferable xn force field reasonably describes the ion pairing that is observed in the UA simulations as a function of sulfonation and temperature. Remarkably, despite eliminating any explicit description of the PEO backbone, the CG model predicts string-like ion aggregates that appear qualitatively consistent with the ionomer peak observed in X-ray scattering experiments and, moreover, with the temperature dependence of this peak.

Introduction

Molecular dynamics (MD) simulations provide tremendous insight into nanoscale structure and interactions. ¹ Unfortunately, all-atom (AA) models do not provide the necessary efficiency for effectively simulating the length and time scales that are relevant for many technologically important phenomena. ² These limitations are particularly apparent for AA simulations of charge conduction in ionomers. Ionomers are polymers with charged groups covalently linked to the polymer backbone. ³ Charge conduction in ionomers is strongly coupled to glassy polymer dynamics ⁴ and, moreover, involves self-assembling ion aggregates that form across nanometer length-scales. ^{5,6} Consequently, although ionomers remain promising candidates for polymer-based batteries, ⁷ AA simulations can only effectively address local aspects of the conduction mechanism. In contrast, by adopting a reduced representation that eliminates unnecessary atomic detail, coarse-grained (CG) models provide the necessary efficiency for investigating mesoscale charge aggregation. ^{8,9} However, in order to realize their promise for designing improved ionomers, CG models must provide predictive accuracy and transferability.

CG models are often developed via top-down or bottom-up approaches. ¹⁰ Top-down models, which are often parameterized to reproduce experimental observables, provide a particularly effective tool for investigating the universal consequences of basic physico-chemical properties. ^{11–13} For instance, simple bead-spring models have investigated the impact of temperature and polymer topology upon charge aggregation in generic ionic polymers. ^{14–17} However, these top-down models lack a direct connection to specific molecular systems and generally provide limited accuracy for describing complex molecular structures. In contrast, bottom-up models, which are parameterized with respect to a high resolution model, can provide the necessary accuracy and chemical specificity for predicting the emergent properties of particular materials. ^{18–20}

In principle, bottom-up models can reproduce the structural and thermodynamic properties of an AA model that are observable at the resolution of the CG model. $^{21-23}$ This

accuracy can be achieved when the CG interactions are modeled with the many-body potential of mean force (PMF), which is a many-body effective free energy function that corresponds to the net Boltzmann weight for the AA configurations that map to a particular CG configuration. ^{24–28} In practice, the PMF cannot be determined for most interesting systems. Nevertheless, systematic coarse-graining methods often approximate the PMF with sufficient accuracy to reproduce simple structural features of a given AA model at the particular state point employed in the parameterization. ^{29–31}

For instance, we have previously developed a very coarse model for characterizing the structure of ionic aggregates that form in a melt of polyethylene-oxide- (PEO-) based ionomer chains. 32 As indicated in Fig. 1 for the case x=1, these ionomer chains consisted of 4 sulfonated isophthalate pendants that were linked by 13 PEO repeats and neutralized by 4 free sodium counterions. Since the relaxation time of the polymer backbone is two orders of magnitude faster than the diffusion of ions, we developed an "ion-only" CG model for investigating ionic aggregates that form in the mean field generated by the polymer matrix. The ion-only CG model explicitly represented the diffusing sodium cations and employed a single site for each sulfonated pendant, but eliminated any explicit description of the PEO backbone. Instead, we implicitly modeled the effects of the polymer backbone with simple pair potentials between the remaining CG sites. By eliminating the explicit polymer environment, the CG model provided sufficient efficiency to simulate ion aggregation for $\approx 8 \text{ ms}$ (as estimated from the simulated diffusion) in a cubic box with sides of $L \approx 15$ nm. ³³ Given this efficiency, the CG simulations can investigate the formation and dissociation of "sticky" ion pairs that are believed important for charge conduction in PEO-based ionomers. ³⁴ Moreover, the CG model can study collective mechanisms for charge transport that have been previously suggested by high resolution simulations. 35 Remarkably, this bottom-up model approximated the many-body PMF with sufficient accuracy to reproduce the ion-ion pair distribution functions that were observed in much shorter ($t_{\rm sim} = 160$ ns) high resolution simulations of much smaller systems ($L \approx 5$ nm). ³²

In this study, we extend this ion-only CG model for multiple chemically distinct ionomers and for multiple temperatures. Because the PMF varies with changes in composition and thermodynamic state point, it remains generally challenging to develop "transferable" CG models. Indeed, many prior studies have investigated the sensitivity of bottom-up models to changes in temperature and density. ^{36–46} Arguably, bottom-up methods have demonstrated even less success for developing transferable potentials that accurately model multiple chemically distinct systems. ^{47–53}

In particular, previous studies have clearly demonstrated the challenge of constructing transferable low-resolution models for highly charged systems. ⁵⁴⁻⁶² As a consequence of eliminating the explicit dielectric environment from the CG representation, the PMF includes important many-body contributions that reflect the polarization of the local environment about a fixed configuration of the charges. ⁵⁴ This entropic component and, thus, the temperature-dependence of the PMF, will systematically increase with coarsening. ⁶³ Although these many-body effects can sometimes be neglected when modeling aqueous salt solutions at a single temperature and sufficiently low charge concentration, ^{55,56} they become increasingly important at salt concentrations above 0.5 M. ⁵⁷ Accordingly, implicit solvent CG models for aqueous salt solutions have often modeled electrostatic interactions with a dielectric constant that varies with either temperature or ion concentration. ^{54,58,59} Of course, this pair-additive mean-field approximation to many-body polarization becomes less reliable at higher salt concentrations. ^{60,61}

While the ion-only CG model shares some similarities with previous implicit solvent models for aqueous charged systems, it also presents important distinct features. For instance, previous implicit solvent CG models averaged over discrete water molecules that relax relatively quickly about a given charge configuration. In contrast, the ion-only model averages over a PEO backbone that is covalently linked to the anionic CG sites. The PEO backbone generates strong steric constraints upon the structure of ionic aggregates that form in the polymer matrix. Additionally, in comparison to the high dielectric and strong

screening of aqueous solutions, the PEO backbone provides a much lower dielectric with reduced screening capability that, moreover, relaxes much more slowly. Consequently, one expects that many-body effects may be even more important for modeling interactions in coarse ionomer models. Furthermore, in comparison to an aqueous environment, the PEO backbone presents a more chemically diverse and heterogeneous environment that can solvate cations with both ether oxygens along the PEO backbone and also bridging carbonyl groups that flank the isophthalate groups. Finally, the ionomer system presents an additional practical challenge, since it is highly nontrivial to obtain sufficient simulated statistics to adequately characterize the sensitivity of the many-body PMF to changes in, e.g., temperature or sulfonation. Thus, one expects it may be particularly challenging to develop transferable potentials for low resolution models of ionomers.

In this work we attempt an "extended ensemble" approach ⁶⁴ to develop transferable potentials for very low resolution CG models of ionomers. Quite generally, we define an extended ensemble as a collection of equilibrium ensembles for chemically distinct systems in multiple thermodynamic state points. ^{65,66} For each ensemble in this collection, we develop a CG potential as an approximation to the corresponding many-body PMF. We construct these approximate potentials by combining simple potentials that govern specific interactions. These simple interaction potentials may be identical across the extended ensemble or, alternatively, they may vary as a function of the thermodynamic state. We determine these interaction potentials via a global variational principle such that, for each ensemble, the combined potential optimally approximates the corresponding many-body PMF. If we perform this variational calculation in a sufficiently large space of approximate potentials, the combined potentials will accurately approximate the many-body PMF for each system and state point within the extended ensemble. Thus, the optimized interaction potentials will be transferable across the extended ensemble. Moreover, one hopes that this transferability will extend to other systems and state points that are governed by "similar physics."

In particular, we consider an extended ensemble that includes 7 different PEO-based

ionomer melts in which varying fractions of the sulfonated isophthalate pendants have been neutralized via hydrolysis. Moreover, we consider each melt at 2 different temperatures. As in our prior ion-only CG model,³² we employ a single site for each cation and each isophthalate group, while eliminating any explicit representation of the PEO backbone. However, we now distinguish between sulfonated and neutralized isophthalate groups.

Of course, this very coarse representation places significant limitations upon the model. For instance, the ion-only model cannot directly probe either the effects of backbone excluded volume upon the structure of ionic aggregates or the role of backbone dynamics for their self-assembly. Nevertheless, the resolution of the ion-only model is sufficient for observing the ion aggregates that form in the polymer matrix. Thus, at least in principle, the many-body PMF exactly describes the effective interactions that govern the structure and statistics of these aggregates. Moreover, the extended ensemble approach provides a principled framework for developing transferable approximations to this PMF. Accordingly, we primarily focus on assessing the accuracy of this extended ensemble approach for modeling the structure and statistics of ion aggregates that form as a function of temperature and ionomer sulfonation.

The remainder of this manuscript is organized as follows. The theory section briefly summarizes the extended ensemble approach and develops the formalism for modeling long-ranged electrostatic interactions with system-dependent effective dielectric constants. The methods section describes the calculation of both system-specific and also transferable potentials for the CG models of ionomers. In particular, this section details the ad hoc procedure adopted for determining the effective dielectric constants. In the results section, we first assess the equilibration of simulations with an optimized united atom (UA) model. ^{6,67,68} We next determine and assess distinct CG potentials for each melt at each temperature. We then determined a single extended ensemble (xn) potential that combined system-independent, short-ranged potentials with long-ranged Coulomb potentials that depend upon system-specific, effective dielectric constants. Our initial estimates of the effective dielectric constants resulted in CG models that accurately modeled the site-site rdfs sampled by the

UA simulations at 398 K, but not at 423 K. However, after revising these dielectric constants, the resulting xn force field reasonably reproduces the site-site rdfs sampled by the UA simulations for the entire extended ensemble. Moreover, simulations with this xn model generate mesoscale aggregates that compare favorably with the "ionomer peak" observed in X-ray scattering experiments. ⁶⁹ The discussion section summarizes the principal results of the study, making connection with previous CG studies, and indicating both the promise and limitations of this approach. Finally, the conclusion section provides closing remarks and outlines future directions for this work.

Theory

In this section, we briefly develop the extended ensemble framework for determining transferable potentials.⁶⁴ In summary, we define an extended ensemble as a collection of equilibrium ensembles for distinct systems under varying thermodynamic conditions. We generalize the multiscale coarse-graining (MS-CG) force-matching⁷⁰ variational principle^{28,71,72} to determine a single set of transferable interaction potentials that, when appropriately combined, provide an optimal approximation to the many-body potential of mean force for each of these equilibrium ensembles. We focus on the treatment of multiple temperatures and electrostatic interactions, since previous applications of this framework have not considered these aspects.⁶⁴⁻⁶⁶

We first define an abstract "topology" variable γ that specifies a high resolution microscopic representation for a particular chemical system. In particular, γ specifies the number, n_{γ} , connectivity, and character of the particles required for a microscopic (e.g., all-atom) description of the system. Further, we assume a classical potential, u_{γ} , that governs the interactions of these particles as a function of the configuration, \mathbf{r}_{γ} . For a given γ and (inverse) temperature, $\beta = 1/k_B T$, we assume that the system configuration, \mathbf{r}_{γ} , samples the

equilibrium canonical distribution:

$$p_{r|\gamma\beta}(\mathbf{r}_{\gamma};\beta) = z_{\gamma:\beta}^{-1} \exp\left[-\beta u_{\gamma}(\mathbf{r}_{\gamma})\right]$$
 (1)

$$z_{\gamma;\beta} = \int d\mathbf{r}_{\gamma} \exp\left[-\beta u_{\gamma}(\mathbf{r}_{\gamma})\right].$$
 (2)

Canonical averages are defined for any observable $a_{\gamma}(\mathbf{r}_{\gamma};\beta)$:

$$\langle a_{\gamma}(\mathbf{r}_{\gamma};\beta)\rangle_{\gamma;\beta} = \int d\mathbf{r}_{\gamma} \, p_{r|\gamma\beta}(\mathbf{r}_{\gamma};\beta) \, a_{\gamma}(\mathbf{r}_{\gamma};\beta)$$
 (3)

In this work, γ identifies the various ionomer melts, while \mathbf{r}_{γ} and u_{γ} indicate the configuration and potential for the corresponding high resolution model.

We next define an "extended ensemble" as a collection of equilibrium canonical ensembles for multiple systems, γ , at one or more temperatures, β . In this work, the combination (γ , β) identifies a simulated ensemble of ionomer system γ at (inverse) temperature β , while the extended ensemble is defined by 13 simulated ensembles selected from simulations of 7 ionomer systems at 2 temperatures. For each combination (γ , β) in the extended ensemble, we assign a fixed weight, $p_{\gamma\beta}$, such that $\sum_{\gamma,\beta} p_{\gamma\beta} = 1$. A microstate of the extended ensemble then specifies a topology, γ , a temperature, β , and a configuration, \mathbf{r}_{γ} , that is sampled with probability

$$p_{\gamma r\beta}(\mathbf{r}_{\gamma};\beta) = p_{\gamma\beta} p_{r|\gamma\beta}(\mathbf{r}_{\gamma};\beta). \tag{4}$$

Extended ensemble averages are evaluated

$$\langle a_{\gamma}(\mathbf{r}_{\gamma};\beta)\rangle = \sum_{\gamma\beta} \int d\mathbf{r}_{\gamma} \, p_{\gamma r\beta}(\mathbf{r}_{\gamma};\beta) \, a_{\gamma}(\mathbf{r}_{\gamma};\beta)$$
 (5)

$$= \sum_{\gamma,\beta} p_{\gamma\beta} \left\langle a_{\gamma}(\mathbf{r}_{\gamma};\beta) \right\rangle_{\gamma;\beta}. \tag{6}$$

In this study we assume a constant volume for each γ and β , although the extended ensemble approach may be readily adapted for systems at constant external pressure.⁶⁶

In order to construct a coarse-grained (CG) representation of the microscopic extended ensemble, we introduce two mapping functions. The topology mapping, μ , determines a CG topology, $\Gamma = \mu(\gamma)$, from an atomic topology, γ . In particular, Γ must specify the number, N_{Γ} , connectivity, and character of the sites in the CG representation. Given the CG representation, $\Gamma = \mu(\gamma)$, the configuration mapping, \mathbf{M}_{γ} , determines a CG configuration $\mathbf{R}_{\Gamma} = \mathbf{M}_{\gamma}(\mathbf{r}_{\gamma})$. We define a "mapped extended ensemble" by mapping each microstate in the microscopic extended ensemble to a CG microstate: $(\gamma, \mathbf{r}_{\gamma}, \beta) \to (\Gamma, \mathbf{R}_{\Gamma}, \beta)$ with $\Gamma = \mu(\gamma)$ and $\mathbf{R}_{\Gamma} = \mathbf{M}_{\gamma}(\mathbf{r}_{\gamma})$. In turn, this determines a weight, $p_{\Gamma\beta}$, for each combination (Γ, β) and a probability, $p_{\Gamma R\beta}(\mathbf{R}_{\Gamma}; \beta)$, for each CG microstate in the mapped extended ensemble:

$$p_{\Gamma\beta} = \sum_{\gamma} p_{\gamma\beta} \, \delta_{\mu(\gamma),\Gamma} \tag{7}$$

$$p_{\Gamma R\beta}(\mathbf{R}_{\Gamma};\beta) = \sum_{\gamma} \int d\mathbf{r}_{\gamma} \, p_{\gamma r\beta}(\mathbf{r}_{\gamma};\beta) \, \Delta_{\gamma;\Gamma}(\mathbf{r};\mathbf{R})$$
 (8)

where we have defined a joint indicator function:

$$\Delta_{\gamma;\Gamma}(\mathbf{r};\mathbf{R}) = \delta_{\mu(\gamma),\Gamma} \,\delta\left(\mathbf{M}_{\gamma}(\mathbf{r}_{\gamma}) - \mathbf{R}_{\Gamma}\right) \tag{9}$$

Note that the mapping preserves the temperature between microstates.

Our objective is to develop a model for a CG extended ensemble that accurately reproduces the statistics of the mapped extended ensemble. This implies that the CG model should weight topologies and temperatures according to

$$P_{\Gamma\beta} = p_{\Gamma\beta} \tag{10}$$

and should sample configurations according to

$$P_{\Gamma R\beta}(\mathbf{R}_{\Gamma};\beta) = p_{\Gamma R\beta}(\mathbf{R}_{\Gamma};\beta). \tag{11}$$

Equation (11) determines (to within a configuration-independent constant) the appropriate CG potential, $W_{\Gamma}(\mathbf{R}_{\Gamma}; \beta)$, for achieving consistency with the mapped extended ensemble:

$$\exp\left[-\beta W_{\Gamma}(\mathbf{R}_{\Gamma};\beta)\right] \propto \sum_{\gamma} p_{\gamma|\Gamma\beta} \int d\mathbf{r}_{\gamma} \, p_{r|\gamma\beta}(\mathbf{r}_{\gamma};\beta) \, \delta\left(\mathbf{M}_{\gamma}(\mathbf{r}_{\gamma}) - \mathbf{R}_{\Gamma}\right) \tag{12}$$

where $p_{\gamma|\Gamma\beta} = p_{\gamma\beta} \, \delta_{\mu(\gamma),\Gamma} / p_{\Gamma\beta}$.

The forces determined from each PMF, $\mathbf{F}_{\Gamma I}^0(\mathbf{R}_{\Gamma};\beta) = -\partial W_{\Gamma}(\mathbf{R}_{\Gamma};\beta)/\partial \mathbf{R}_{\Gamma I}$, equal conditioned averages of the fluctuating atomic forces experienced by the CG sites, $\mathbf{f}_{\gamma I}(\mathbf{r}_{\gamma})$, when averaged over the high resolution microstates $(\gamma, \mathbf{r}_{\gamma}, \beta)$ that map to $(\Gamma, \mathbf{R}_{\Gamma}, \beta)$:

$$\mathbf{F}_{\Gamma I}^{0}(\mathbf{R}_{\Gamma};\beta) = \left\langle \mathbf{f}_{\gamma I}(\mathbf{r}_{\gamma}) \right\rangle_{\mathbf{R}_{\Gamma};\beta}$$
(13)

where

$$\langle a_{\gamma}(\mathbf{r}_{\gamma};\beta) \rangle_{\mathbf{R}_{\Gamma};\beta} = \sum_{\gamma} \int d\mathbf{r}_{\gamma} \ p_{\gamma r|\Gamma R\beta}(\mathbf{r}_{\gamma}|\mathbf{R}_{\Gamma};\beta) \ a_{\gamma}(\mathbf{r}_{\gamma};\beta)$$
 (14)

$$p_{\gamma r|\Gamma R\beta}(\mathbf{r}_{\gamma}|\mathbf{R}_{\Gamma};\beta) = p_{\gamma r\beta}(\mathbf{r}_{\gamma};\beta) \Delta_{\gamma;\Gamma}(\mathbf{r};\mathbf{R}) / p_{\Gamma R\beta}(\mathbf{R}_{\Gamma};\beta).$$
 (15)

Thus, W_{Γ} is a generalized many-body potential of mean force (PMF).

In practice, we cannot determine or simulate W_{Γ} . Instead, our objective is to determine, for each combination (Γ, β) in the mapped ensemble, a potential, $U_{\Gamma}(\mathbf{R}_{\Gamma}; \beta)$, that optimally approximates the corresponding PMF, $W_{\Gamma}(\mathbf{R}_{\Gamma}; \beta)$. For this purpose, we adopt an extended ensemble force-matching variational principle.^{28,73} Given a set of approximate potentials for the extended ensemble, $U \equiv \{U_{\Gamma}(\mathbf{R}_{\Gamma}; \beta)\}$, we define

$$\chi^{2}[U] = \left\langle \frac{1}{3N_{\mu(\gamma)}} \sum_{I \in \mu(\gamma)} \left| \mathbf{f}_{\gamma I}(\mathbf{r}_{\gamma}) - \mathbf{F}_{\mu(\gamma)I}(\mathbf{M}_{\gamma}(\mathbf{r}_{\gamma}); \beta) \right|^{2} \right\rangle$$
(16)

where $\mathbf{F}_{\Gamma I}(\mathbf{R}_{\Gamma};\beta) = -\partial U_{\Gamma}(\mathbf{R}_{\Gamma};\beta)/\partial \mathbf{R}_{\Gamma I}$. It follows from Eq. (13) that ^{28,64}

$$\chi^2[U] = \chi^2[W] + \left| \left| \mathbf{F} - \mathbf{F}^0 \right| \right|^2, \tag{17}$$

where $W \equiv \{W_{\Gamma}(\mathbf{R}_{\Gamma}; \beta)\}$ and

$$\left|\left|\mathbf{F} - \mathbf{F}^{0}\right|\right|^{2} = \sum_{\Gamma,\beta} \int d\mathbf{R}_{\Gamma} \, p_{\Gamma R\beta}(\mathbf{R}_{\Gamma};\beta) \frac{1}{3N_{\Gamma}} \sum_{I \in \Gamma} \left|\mathbf{F}_{\Gamma I}(\mathbf{R}_{\Gamma};\beta) - \mathbf{F}_{\Gamma I}^{0}(\mathbf{R}_{\Gamma};\beta)\right|^{2} \ge 0. \tag{18}$$

Thus, the global minimum of χ^2 determines $W_{\Gamma}(\mathbf{R}_{\Gamma}; \beta)$ to within a term that is configuration-independent for each combination (Γ, β) in the extended ensemble. Accordingly, given a parametric form for CG potentials in the extended ensemble, we can determine the optimal parameters for approximating W_{Γ} by minimizing χ^2 . The extended ensemble variational principle simply reduces to the conventional MS-CG variational principle when only a single system and temperature are included in the extended ensemble.

Our objective is to construct a set of tractable CG potentials $U_{\Gamma}(\mathbf{R}_{\Gamma}; \beta)$ that accurately approximate $W_{\Gamma}(\mathbf{R}_{\Gamma}; \beta)$ for the range of compositions, Γ , and temperatures, β , within (and hopefully outside) the mapped extended ensemble. One can envision many strategies for constructing such approximations. For instance, one might attempt to define the approximate potentials, U_{Γ} , as a sum of transferable, i.e., system-independent, potentials:

$$U_{\Gamma 0}(\mathbf{R}_{\Gamma}) = \sum_{\zeta} \sum_{\lambda \in \Gamma} U_{\zeta}(\psi_{\zeta}(\mathbf{R}_{\Gamma \lambda})). \tag{19}$$

In Eq. (19), $U_{\zeta}(x)$ is a transferable interaction potential governing a single type of interaction, e.g., a particular nonbonded interaction, that depends upon a scalar function, ψ_{ζ} , of the coordinates, $\mathbf{R}_{\Gamma\lambda}$ for a particular subset, λ , of CG sites in the CG topology, Γ . In this case, $U_{\Gamma 0}$ is independent of temperature and depends upon Γ only via the particular set of interactions that are present in the system. Each interaction potential, U_{ζ} , is then represented by a set of simple basis functions, 73,74 e.g., linear splines, with coefficients, ϕ_{ζ} , that are

independent of Γ and β .

However, this simple transferable approximation, $U_{\Gamma 0}(\mathbf{R}_{\Gamma})$, proved inadequate for reproducing the temperature dependence of charge association in the ionomers. As a next approximation, we introduced an additional Coulombic potential to model long-ranged electrostatic interactions:

$$U_{\Gamma 1}(\mathbf{R}_{\Gamma}; \beta) = \sum_{(I,J)\in\Gamma} \frac{q_I q_J}{4\pi\epsilon_0 \ \epsilon_{\Gamma\beta} R_{IJ}}$$
 (20)

In Eq. (20), q_I and q_J are the charges of sites I and J, R_{IJ} is the distance between the pair, ϵ_0 is the permittivity of free space, and $\epsilon_{\Gamma\beta}$ is an effective dielectric that explicitly varies with both the composition, Γ , and also the temperature, β , of the system. In principle, $\epsilon_{\Gamma\beta}$ may be optimized via variational calculation, although we did not adopt this approach. Instead, we determined $\epsilon_{\Gamma\beta}$ by ad hoc methods that are described in the Methods and Results sections. Given $\epsilon_{\Gamma\beta}$, the approximate potential was then defined:

$$U_{\Gamma}(\mathbf{R}_{\Gamma}; \beta; \boldsymbol{\phi}) = U_{\Gamma 0}(\mathbf{R}_{\Gamma}; \boldsymbol{\phi}) + U_{\Gamma 1}(\mathbf{R}_{\Gamma}; \beta). \tag{21}$$

This potential may be optimized by minimizing χ^2 with respect to the system-independent parameters, $\boldsymbol{\phi}$, while treating the Coulomb potential, $U_{\Gamma 1}(\mathbf{R}_{\Gamma}; \beta)$, as a fixed reference potential. ^{73,75} Since the transferable interaction potentials $U_{\zeta}(x; \boldsymbol{\phi}_{\zeta})$ depend linearly upon the potential parameters, $\boldsymbol{\phi}_{\zeta}$, minimizing χ^2 reduces to a linear least squares problem and the optimal parameters are determined from the linear system of equations ^{73,76}

$$\sum_{D'} G_{DD'} \phi_{D'} = b_D \tag{22}$$

where $G_{DD'}$ is a matrix of extended ensemble averages describing the relevant many-body correlations and b_D is an array describing the fluctuating atomic forces that are not accounted for by the reference potential, $U_{\Gamma 1}$. ^{73,75} As in our prior ionomer study, ³² we solved this linear system of equations by employing a generalized-Yvon-Born-Green theory ^{64,77,78} to determine

the force vector b_D from appropriate structural correlations.

Methods

Ionomer systems

We considered 7 different ionomer melts, each containing 27 chains. As illustrated in Fig. 1, each chain consisted of 4 isophthalate groups, i.e., a benzene ring flanked by two carbonyl groups, that were connected by 13 polyethylene oxide (PEO) repeats, i.e., $-(CH_2CH_2O)_{13}-$. These isophthalate groups may be either neutral or charged. The charged groups were modified by covalent attachment of a sulfate anion to the benzene ring at the second carbon with respect to either carbonyl group. We simulated systems in which 25, 38, 50, 63, 75, 83, or 100 % of the isophthalate groups were sulfonated. For systems with incomplete sulfonation, the sulfonation sites were randomly selected, i.e., the systems are polydiverse. In each case, sodium ions were added to ensure charge neutrality of the system.

High resolution models and simulations

Maranas and coworkers have previously performed high resolution simulations for each of these ionomer melts at several different temperatures, 68 while using an optimized united atom (UA) potential. Notably, this UA potential employed reduced charges for each ionic group in order to provide a realistic description of the dynamics observed in quasi-elastic neutron scattering experiments. After a 200 ns equilibration period, each simulation was continued for an additional 1 μ s, during which configurations were sampled every 10 ps. We employed the resulting 10⁵ simulated UA configurations to construct and assess CG models for each melt at two different temperatures, T = 398 K and 423 K.

CG Models and Simulations

In the following, we present results for both system- (and temperature-) specific and also transferable CG models. The CG models employ the same low resolution representation and the same molecular mechanics form for the interaction potential. The models differ in their parameterization and in their treatment of long-ranged electrostatic interactions.

Mapping

As illustrated in Fig. 1, we represented each polymer with 4 CG sites, while employing 3 distinct types of sites. We represented sulfonated isopthalate groups with "S" sites that correspond to the sulfur atom of the corresponding sulfate anion. We represented neutral isopthalate groups with "C" sites that correspond to the second carbon with respect to either carbonyl group. Finally, we represented sodium cations with "Na" sites. The remaining atoms in the system, including the atoms of the PEO backbone, were eliminated from the CG representation.

Approximate potentials

The CG models employed a simple molecular mechanics potential with separate bonded and nonbonded contributions. In particular, the CG models employed a bond potential between consecutive sites along the polymer chain to mimic the connectivity of the PEO linkers. The same bond potential was employed for each pair of consecutive bonded sites, irrespective of whether they corresponded to sulfonated or neutralized isophthalate groups. The CG models did not employ angle or torsion potentials. The nonbonded potential employed central pair potentials to model the interactions between each pair of sites. We determined a distinct pair potential for each distinct pair of site types. We did not exclude "bonded" pairs from the nonbonded potential, i.e., consecutive sites along the polymer backbone interacted via both bonded and nonbonded potentials. We emphasize that the potential does not include terms to explicitly describe the excluded volume of the polymer backbone and, consequently,

does not prevent "crossing" of the chains. Rather, the potential approximates the effective interactions between the CG sites in the presence of the mean field generated by the polymer backbone and surrounding matrix.

We parameterized both specific MS-CG and transferable extended ensemble (xn) CG force fields for the ionomer systems. In both cases, we represented all calculated force functions with linear spline basis functions, while employing a grid spacing of 0.02 nm and 0.05 nm for bonded and nonbonded forces, respectively. We employed a cutoff of 2.4 nm for modeling short-ranged nonbonded interactions. Since the effective bonds between consecutive isophthalate groups occasionally extended across more than half of the UA simulation box, we constructed a larger super-cell when calculating the CG force field. This super-cell included 27 periodic images of the original UA simulation box that were arranged as a cube. This super-cell reflects the relatively modest size of the original UA simulation box and the relatively extended nature of the polymer conformations. It is possible that the statistics of the UA simulations might reflect resulting finite size effects. We expect these finite size effects to be modest, though, since the PEO backbone appears to introduce only weak correlations between successive isophthalate groups. It is also the case that CG potentials can suffer from significant finite size effects that preclude their transferability to system sizes different from the original high resolution simulation. ⁷⁹ However, the use of the supercell for calculating the CG potentials did not appear to introduce additional finite size effects into the CG model, since (1) we obtained similar CG potentials for different treatments of the periodic boundaries; and (2) these CG potentials provide similar accuracy for different system sizes with the same density.

From this super-cell, we determined the relevant ensemble averages for calculating the CG force field parameters. In particular, we employed the g-YBG theory to determine the relevant force averages, b_D , from appropriate structural correlations.^{75,77,80} In order to make these calculations more robust, we performed certain modifications to the normal equations that we have previously discussed.⁸¹ We then solved the resulting system of linear equations

via singular value decomposition after applying right-left preconditioning to make the matrix dimensionless.

We employed the calculated parameters to generate GROMACS table files for subsequent simulations. ⁸² In this process, we linearly extrapolated the calculated force functions into regions that were not sampled during the UA simulations. In particular, we extrapolated both the bonded and non-bonded pair potentials into the short-ranged "hard core" region in order to ensure the excluded volume of the sites. Similarly, we extrapolated the bond potential at large bond lengths in order to ensure the integrity of the CG bond. Although generally successful, this automated procedure occasionally introduced very minor artifacts at the boundaries of the calculated potentials, as demonstrated below and detailed in the Supporting Information.

System-specific MS-CG force fields

We employed the MS-CG variational principle ^{28,71,72} to independently parameterize a distinct CG force field for each polymer system at each temperature. These models did not treat explicit electrostatic interactions, but instead employed short-ranged pair potentials for treating all non-bonded interactions.

Transferable extended ensemble force field

With the exception of the fully sulfonated ionomer melt at T=398 K, the extended ensemble included all 7 melts at both temperatures. We employed the extended ensemble variational principle ⁶⁴ to determine a single transferable force field for modeling the entire extended ensemble. Each of the 13 remaining UA simulations was given equal weight in performing this variational calculation, i.e., $p_{\gamma\beta}=1/13$ for these 13 ensembles.

The transferable extended ensemble (xn) force field modeled bonded and short-ranged non-bonded interactions with the same potential functions for each system and temperature. This force field also included Coulomb potentials, U_C , to model long-ranged electrostatic

interactions, while employing an effective dielectric, $\epsilon_{\Gamma\beta}$, that varied with both system, Γ , and temperature, β :

$$U_{C;IJ}(R_{IJ}) = q_I q_J / 4\pi \epsilon_0 \epsilon_{\Gamma\beta} R_{IJ} . \qquad (23)$$

For consistency with the UA simulations, ^{6,68} we assigned a charge of +0.5e and -0.5e to each Na and S site, respectively. We adopted the following ad hoc approach to determine a simple analytic form for the system-specific dielectrics.

We first employed the MS-CG potentials to determine an initial estimate for the systemspecific effective dielectrics. For each combination (Γ,β) , we determined $\epsilon_{\Gamma\beta}$ such that Coulomb potentials most accurately fit the system-specific MS-CG pair potentials for the Na-Na, Na-S, and S-S interactions at large distances, i.e., over the interval $R_{lr} < R < R_{cut}$. The cut-off, $R_{cut} = 2.4$ nm, corresponded to the range employed in calculating the MS-CG potentials. However, the fits depended quite sensitively upon R_{lr} . We tentatively defined $R_{lr} = 1.5$ nm, such that the resulting effective dielectrics agreed qualitatively with the experimentally measured value for the dielectric of the unsulfonated polymer. ^{4,69}

We next fit these estimated dielectrics, $\epsilon_{\Gamma\beta}$, to the analytic form:

$$\epsilon_{\text{eff}}(C, T; A, b) = A (T/T_0)^{-1} \exp[-b C],$$
 (24)

in which T is the temperature, $T_0 = 398$ K, and the ion content is defined $C = n_{\text{Na}}/(n_{\text{Na}} + n_{\text{EO}})$, where n_{Na} and n_{EO} are, respectively, the number of sodium ions and ether oxygens in the system. The T^{-1} dependence for the dielectric was motivated by the dielectric response of independent dipoles, while the exponential dependence upon C was inferred empirically. Given the functional form in Eq. (24), along with the dielectrics estimated from the system-specific MS-CG potentials, we determined the two free parameters: $A_0 = 9.75$ and $b_0 = 6.23$.

We defined a system-specific reference Coulomb potential for each combination (Γ, β) by setting $\epsilon_{\Gamma\beta} \equiv \epsilon_{\text{eff}}(C_{\Gamma}, T_{\beta}; A_0, b_0)$ where C_{Γ} is the ion content for system Γ and $T_{\beta} =$ $(k_B\beta)^{-1}$. Given these system-specific Coulomb potentials as a fixed reference potential, 73,75 we employed the extended ensemble variational principle to determine system-independent potentials, $U_{\zeta;xn}(R)$, for modeling bonded and short-ranged nonbonded interactions. Since our initial estimates of the system-specific dielectrics depended quite sensitively upon R_{lr} , we employed the resulting transferable potentials to obtain a more robust estimate for $\epsilon_{\Gamma\beta}$. For each (Γ, β) in the extended ensemble, we subtracted the transferable xn short-ranged potential, $U_{\zeta;xn}(R)$, from the corresponding system-specific MS-CG pair potential, $U_{\zeta;\Gamma\beta}(R)$, in order to obtain an improved estimate of the electrostatic contribution to the system-specific MS-CG pair potential for the Na-Na, Na-S, and S-S interactions:

$$U_{\zeta;\Gamma\beta}^{\rm el}(R) \equiv U_{\zeta;\Gamma\beta}(R) - U_{\zeta;\rm xn}(R). \tag{25}$$

When fit to the Coulomb form, the resulting potentials, $U_{\zeta;\Gamma\beta}^{\rm el}(R)$, provided a more robust estimate of $\epsilon_{\Gamma\beta}$ for each pair (Γ, β) . We then fit the revised dielectrics to Eq. (24), to obtain $A_1 = 16.8$ and $b_1 = 10.9$. These parameters determined a new effective dielectric for each pair $\epsilon_{\Gamma\beta} \equiv \epsilon_{\rm eff}(C_{\Gamma}, T_{\beta}; A_1, b_1)$.

We obtained a single force field for modeling the entire range of systems and compositions by combining the resulting long-ranged Coulomb potentials, $U_{\Gamma 1}$, with the transferable bonded and short-ranged non-bonded potentials, $U_{\Gamma 0}(\mathbf{R}_{\Gamma}; \boldsymbol{\phi})$. However, this force field did not reproduce the temperature-dependence observed in the UA simulations for the site-site rdfs. By performing additional studies, we determined that this temperature variation was quite accurately reproduced when the dielectric constants at T = 423K were heuristically rescaled by 0.8. Accordingly, we finally modeled the dielectrics with the functional form:

$$\epsilon_{\text{eff}}(C, T) = A \left(T/T_0 \right)^{-\alpha} \exp\left[-b C \right], \tag{26}$$

with $\alpha = 4.66$, $A = A_1$ and $b = b_1$. This expression was adopted for determining the electrostatic contributions to the final transferable CG force field, i.e., the xn-s force field.

Note that we employed the same bonded and short-ranged nonbonded pair potentials in all versions of the transferable xn force field. In particular, we did not reoptimize these transferable potentials for consistency with the revised effective dielectrics.

CG simulations

We employed Gromacs 4.5.3 to simulate all CG models in the constant NVT ensemble, ⁸² while employing the stochastic dynamics algorithm ⁸⁴ with a friction coefficient of 2.0 ps⁻¹. In particular, we employed a 1 fs time step for the CG simulations, although our previous studies employed time steps of up to 4 fs without any apparent negative numerical consequences. ³² We performed all CG simulations in the extended super-cell used for calculating the CG force field. We modeled electrostatic interactions for the transferable xn force field with the particle mesh Ewald method, ⁸⁵ while employing a Fourier grid spacing of 0.08 nm. We employed a cutoff of 2.4 nm both for short-range nonbonded interactions and for the real-space contribution to electrostatic interactions. Table I provides additional details regarding the CG simulations.

We determined the initial configuration for each simulation by mapping, to the CG representation, a configuration from the final quarter of the corresponding UA simulation. Starting from this initial configuration, we first performed an energy minimization according to the corresponding CG potential. We then simulated the resulting configuration for 5.5×10^6 time steps. After discarding the first 5×10^5 steps for equilibration, we sampled every $1000^{\rm th}$ configuration in order to obtain 5×10^3 configurations for subsequent analysis.

Results

We consider CG models of 7 PEO-based ionomer melts with varying degrees of sulfonation at T=398 K and 423 K. Table I describes the composition of these melts and their CG representations. As illustrated in Fig. 1, the CG models explicitly represent each diffusing

sodium cation with a "Na" site, while representing the charged polymers with much reduced resolution. We represent each sulfonated isophthalate group with an "S" site and each hydrolyzed isophthalate group with a "C" site. As in our prior work, we eliminate the PEO-linkers from the CG representation and model their effects implicitly via the effective potentials that govern the interactions between the remaining CG sites.

In the following, we first assess the convergence of statistics obtained from high resolution ionomer simulations. We next construct and assess a system-specific MS-CG potential for each ionomer system and temperature. We then develop and assess a single transferable CG potential for modeling the entire range of ionomer systems and both temperatures. Finally, we briefly investigate the mesoscale ionic aggregates that form in simulations with the resulting model. We explicitly present results for melts with 25, 50, 75, and 100% sulfonation. The Supporting Information demonstrates that similar results are obtained for the other 3 melts.

Equilibration

Maranas and coworkers previously simulated these ionomer systems at several different temperatures ⁶⁸ with an optimized united atom (UA) model. ⁶ Before parameterizing the CG models, we first investigated the sampling provided by these UA simulations. The extended ensemble theory requires particularly rigorous statistical sampling, since the mapped UA ensembles must quantify the sensitivity of the many-body PMF to changes in sulfonation and temperature.

We first considered a time-dependent ion-pairing probability function 33

$$P_2(\tau) = N^{-1} \sum_{i=1}^{N} \langle I_i(t, t+\tau) \rangle_t,$$
 (27)

which quantifies the probability that an ion-pair is coordinated at a given time t and also at a later time $t + \tau$. In Eq. (27), the sum is performed over the N ions in the UA simulation,

the subscripted angular brackets indicate a time average over the sampled configurations, and $I_i(t, t + \tau)$ is an indicator function: $I_i(t, t + \tau) = 1$ if ion i is coordinated with exactly the same counter-ion at times t and $t + \tau$; otherwise $I_i(t, t + \tau) = 0$.

Figure 2 demonstrates that $P_2(\tau)$ displays characteristic behavior on several different time scales. At $\tau = 0$, $P_2(\tau)$ is the probability that an ion is paired in a single sampled configuration. At short times, $P_2(\tau)$ decays exponentially due to the activation barrier for the ion-pair to separate. On slightly longer time scales, the cations diffuse randomly through increasingly large volumes $V(\tau) \sim \tau^{3/2}$, which leads to a probability, $P_2(\tau) \sim \tau^{-3/2}$, for the pair to re-combine. Finally, for $\tau \geq \tau_{\infty}$, $P_2(\tau)$ fluctuates about $P_{\infty} \equiv P_2(0)^2/(N/2)$, which is the probability that any two uncorrelated counter-ions are paired to one another. Consequently, τ_{∞} quantifies the time scale for a cation to become completely uncorrelated from its initial partner and diffuse through the entire simulated volume. Figure 2 demonstrates that $\tau_{\infty} \approx 10-100$ ns for most of the UA simulations. Indeed, the simulated mean square displacements indicate that the sodium cations become diffusive on this time scale. (See Supporting Figures S1 and S2.) Thus, Fig. 2 suggests that, with the possible exception of the completely sulfonated ionomer system at T = 398K, the UA simulations provide equilibrium statistics for ion-pairing in all systems at both temperatures. Moreover, block analysis of the simulated ion-pair rdfs from the UA simulations leads to similar conclusions. Accordingly, with the exception of this most slowly equilibrating system, we included all of the simulated melts in the extended ensemble for parameterizing the transferable CG models.

In addition, we also investigated the convergence of statistics for the polymer conformations. In contrast to the cations, Figs. S1 and S2 indicate that the anions along the polymer backbone do not demonstrate diffusive dynamics on the timescale of the UA simulations. The Supporting Information (SI) also demonstrates that the polymer radius of gyration systematically increases during the early stages of the 1 μ s production simulation with the UA model. This additional "burn-in" time is typically on the order of 100 ns and ranges from approximately 20 ns (T = 423 K, 38% sulfonation) to 700 ns (T = 398 K, 83% sulfonation), while generally decreasing with increasing temperature and decreasing sulfonation. Nevertheless, the SI suggests that, after this additional equilibration period, the polymer radius of gyration samples a steady state distribution during the remainder of the UA simulations. Consequently, in the following, we present only tentative qualitative comparisons between the polymer conformations sampled in the UA and CG models.

Calculated MS-CG potentials

We employed the g-YBG method^{77,80} to parameterize a distinct MS-CG model^{28,71,72} for each ionomer system at each temperature. These MS-CG models employed short-ranged pair potentials to describe all non-bonded interactions, i.e., the CG sites did not have explicit charges. Additionally, for each system and temperature, the MS-CG model employed a single potential for describing all bonds. The models did not include angle or torsion potentials. Figures 3 and 4 present a subset of the calculated MS-CG bonded and nonbonded pair potentials, respectively. The Supporting Information presents all of the calculated potentials.

The MS-CG bond potentials demonstrate a very strong repulsive force at short distances and, at longer distances, a soft anharmonic restoring force that extends over several nanometers. With the exception of the fully sulfonated system at $T=423~\rm K$, each bond potential demonstrates a very shallow "coordination minimum" at $r_b\approx 0.5~\rm nm$ that likely corresponds to the PEO linker bending as consecutive isophthalate groups coordinate the same cation. At $T=398~\rm K$, the restoring potentials appear very similar for all systems except the fully sulfonated system, which likely reflects the slow convergence observed in Fig. 2. At $T=423~\rm K$, the restoring potentials systematically soften with increasing sulfonation. Moreover, the coordination minimum of the bond potential becomes progressively more shallow with increasing sulfonation and completely disappears for the fully sulfonated polymer. Finally, note that the bond potential for completely sulfonated ionomers at $T=423~\rm K$ demonstrates the extrapolation of the bonded potentials for bond lengths that were not sampled in the UA simulations.

The system- (and temperature-) specific MS-CG models employ 6 distinct pair potentials to model the non-bonded interactions between C, S, and Na sites. The left column of Fig. 4 presents the C-C, S-Na, and S-S pair potentials that were calculated at T=398K, while the right column demonstrates the temperature variation in these potentials at short distances. The C-C pair potentials possess a shallow minimum and vary only weakly with changes in temperature or sulfonation, although it appears that they become slightly less attractive with sulfonation. In contrast, the pair potentials for the charged sites reflect much stronger electrostatic interactions and vary more dramatically between systems. In particular, the S-Na pair potential reflects strong electrostatic attraction and, moreover, becomes increasingly attractive with increasing sulfonation and temperature. Conversely, the S-S pair potential is purely repulsive and becomes increasingly repulsive with increasing sulfonation and temperature. Thus, the MS-CG pair potentials suggest that the effective dielectric between the sites decreases with increasing sulfonation and temperature.

Assessment of MS-CG models

We simulated each ionomer system at each temperature with the corresponding optimized MS-CG potential. Figure 5 compares the conformations sampled by ionomers in the simulated MS-CG ensembles (dashed curves) and in the mapped UA ensembles (solid curves), i.e., the ensembles generated by mapping the sampled UA configurations to the CG representation. It is important to appreciate that these conformations must be compared at the resolution of the CG model. In particular, the CG "bonds" do not correspond to chemical bonds between atoms or even to the length of the PEO linkers between isophthalate groups, but rather to the distance between particular atoms (either C or S) of successive isophthalate groups in the UA model. Similarly, we employ the same atoms when comparing the radius of gyration sampled by the mapped UA and simulated MS-CG ensembles.

The mapped and simulated CG ensembles demonstrate extremely broad bond distributions with a dominant peak near $r_b = 2$ nm. The distributions also demonstrate smaller peaks at very short bond length, $r_b \approx 0.5$ nm, which correspond to the coordination minima of the bond potentials in Fig. 3. These peaks grow slightly with increasing concentration of cations.

The MS-CG models qualitatively reproduce the distributions of bond lengths sampled in the mapped UA ensembles. In particular, the MS-CG models reasonably reproduce the general shape of the distributions and, in most cases, the probability for consecutive bonded sites to solvate the same cation. Additionally, in both the UA and MS-CG models, the CG bond distributions shift to larger distances with increasing temperature. However, the MS-CG distributions slightly overestimate the average bond length and also demonstrate a pronounced shift with increasing sulfonation that is not observed in the UA distributions. Finally, Fig. 5a also demonstrates a minor artifact at very long bond lengths $r_b > 3.6$ nm, which is due to the (overestimated) extrapolation of the MS-CG bonded potentials in Fig. 3.

Figure 5b compares distributions for the radius of gyration, R_g , in the mapped and simulated CG ensembles. As described in the SI, the UA distributions have been sampled after R_g appears to have achieved a steady state distribution, since the polymer conformations equilibrate rather slowly in the UA simulations. The UA simulations sample relatively broad distributions for R_g . At $T=398\mathrm{K}$ these distributions do not demonstrate any obvious trend with sulfonation. At $T=423\mathrm{K}$ they shift to slightly larger R_g and are quite insensitive to sulfonation. In contrast, the MS-CG models sample slightly larger conformations that are characterized by narrow Gaussian distributions and, moreover, demonstrate simple variation with sulfonation and temperature. Interestingly, in the MS-CG models, the ionomers expand as electrostatic interactions become increasingly strong with increasing sulfonation and temperature.

Clearly, the MS-CG models do not accurately reproduce the mapped ensemble distributions for the polymer radius of gyration. While the MS-CG distributions are almost certainly well converged, it is possible that the UA simulations are not sufficiently long to adequately sample the equilibrium distribution for such a large scale property, especially at T = 398K. However, it is also quite likely that, given the extremely coarse representation, the simple approximate CG potentials cannot adequately describe the physical forces that govern the ionomer size distribution. Consequently, we will focus on ion pairing statistics in the following, since our primary interest is in the formation of mesoscale charge aggregates, rather than in details of the polymer conformations.

The top and bottom rows of Fig. 6 present the S-Na and S-S site-site radial distribution functions (rdfs), respectively, for the mapped UA and simulated MS-CG ionomer ensembles. We do not present the Na-Na and C-X rdfs here, since they provide little additional insight. The Na-Na rdfs mirror the trends in the S-S rdfs, although we note that the MS-CG models describe the Na-Na rdfs with slightly reduced accuracy. Conversely, the C-X rdfs demonstrate only modest variation with temperature and sulfonation and, moreover, the MS-CG models accurately reproduce these rdfs. The Supporting Information presents a complete comparison of the UA and MS-CG rdfs.

The S-Na rdfs demonstrate a large peak that describes the solvation of Na cations by anionic isophthalate groups. The maximum and shoulder of this peak correspond to different orientations between the isophthalate group and free Na cation. The S-S rdfs feature a smaller broad peak at greater distance that presumably corresponds to multiple isophthalate groups solvating the same cation. At a given temperature, the S-Na rdf peak systematically decreases with increasing sulfonation, while the S-S rdf peak demonstrates the opposite trend. Conversely, both the S-Na and S-S rdf peaks increase with increasing temperature, as a consequence of the increasing stability of larger ionic aggregates.

The system-specific MS-CG models quite accurately reproduce the UA site-site rdfs. The largest discrepancies occur when the ionomer is least sulfonated. In this case, the MS-CG model underestimates the ion-pairing that is observed in the UA simulations at both temperatures. Nevertheless, the MS-CG models reproduce the position and, usually, the heights of the peaks in the mapped site-site rdfs.

In order to further quantify the effective attraction between oppositely charged ions, Fig. 7

presents the integral $I = \int \mathrm{d}r \ 4\pi r^2 g_{\mathrm{S-Na}}(r)$ integrated over the first peak of the rdf. This integral quantifies an effective association constant for ion-pairing ⁸⁶ and is closely related to the number of isophthalate groups coordinating each cation. The MS-CG models reproduce the effective ion-pairing attraction of the UA model quite accurately. More importantly, the MS-CG models accurately describe the sensitivity of this effective attraction to both sulfonation and temperature. Thus, as previously observed, ³² the MS-CG models appear to provide a reasonably accurate description of the ion-pairing tendencies of an optimized UA model for PEO-based ionomers.

Construction of xn potentials

We next employed the extended ensemble framework 64 in order to determine transferable potentials for modeling the entire range of ionomer systems and temperatures. (As noted above, we did not include the completely sulfonated system at T=398K in the extended ensemble.) We initially attempted to determine a single set of transferable short-ranged pair potentials for modeling nonbonded interactions across the entire extended ensemble. However, the resulting models did not satisfactorily reproduce the trends in the UA site-site rdfs. Consequently, we represented the nonbonded potential with both transferable short-ranged potentials and also long-ranged Coulomb potentials between the charged CG sites. These Coulomb potentials employed system- (and temperature-) dependent effective dielectric constants to mimic the dielectric environment eliminated from the CG representation. Note that these effective dielectrics reflect the reduced charges adopted in the UA model and also in the transferable CG force field.

In principle, the extended ensemble variational principle may be used to determine the effective dielectric for each system and temperature. However, as detailed in the Methods section, we instead adopted the following ad hoc procedure. We first tentatively estimated the effective dielectric for each UA simulation by fitting the tails of the corresponding MS-CG potentials. This fitting was confounded by noise in the calculated MS-CG potentials

and demonstrated significant sensitivity to the fitting parameters. Nevertheless, in order to develop a predictive model for the effective dielectric, we fit these estimated dielectrics to the functional form $\epsilon_{\text{eff}} = A(T/T_0)^{-1} \exp{[-bC]}$, where A and b are fit parameters, T is the temperature, $T_0 = 398\text{K}$, and C is the ion content. Figure 8a presents the estimated effective dielectrics and the resulting analytic fit. As suggested by Figs. 4, 6, and 7, the effective dielectric systematically decreases with both temperature and with sulfonation.

We employed this analytic expression to determine a reference Coulomb potential for each ionomer system at each temperature. Given these reference Coulomb potentials, we then employed the extended ensemble variational principle to determine transferable bond potentials and short-ranged nonbonded pair potentials. Figure 9 presents the resulting transferable bond potential, while Fig. 10 presents the resulting transferable short-ranged nonbonded pair potentials.

The extended ensemble (xn) bond potential demonstrates many features observed in the system-specific MS-CG bond potentials, including the rapidly varying repulsive force at contact, the shallow minima at $r_b \approx 0.5$ nm, and also the soft anharmonic restoring force at larger bond lengths. Figure 9b demonstrates that, at longer extensions, the corresponding bond force agrees quite well with the Langevin model⁸⁷ for the end-to-end distance, R, of a freely jointed chain of N Kuhn monomers each of length b under constant tension, $F_b(R) \equiv +\mathrm{d}U_b(R)/\mathrm{d}R$:

$$\langle R \rangle = R_0 + bN \left[\coth \left(\beta b F_b \right) - \left(\beta b F_b \right)^{-1} \right]$$
 (28)

where $R_0 = 0.776$ nm is a shift that corresponds to consecutive anions solvating the same cation, b = 1.163 nm matches well with the Kuhn length of the PEO linker ($b_{\text{PEO}} = 1.18$ nm) that has been inferred from experiments, ⁸⁸ N = 3.63 agrees well with the expected number of Kuhn monomers in the PEO linker, and β is the inverse temperature at T = 410.5K, which is the average of the two temperatures employed in the extended ensemble. Thus,

the extended ensemble method appears to determine a physically reasonable potential for modeling the pseudo-bond between consecutive CG sites along the chain.

Figure 10a presents the transferable xn short-ranged nonbonded pair potentials that involve the neutral C site. The MS-CG pair potentials for the C site demonstrate little variation with sulfonation or temperature, as illustrated in Fig. 4 and in the Supporting Information. Consequently, the xn short-ranged pair potentials for the C site are very similar to the corresponding MS-CG potentials. Nevertheless, the xn potentials for C-X interactions are not simple averages of MS-CG potentials.

Figure 10b presents the transferable xn short-ranged potentials for the charged Na and S sites. In comparison to the system-specific MS-CG potentials presented in Fig. 4, the short-ranged xn potentials are considerably weaker and decay more rapidly. Moreover, these xn potentials change sign with distance. Nevertheless, the short-ranged xn potentials appear to retain some electrostatic character. For instance, the S-Na potential is almost exclusively attractive and is, moreover, much more attractive than other short-ranged xn potentials. Thus, it appears that the decomposition of the non-bonded pair potentials with the system-specific dielectric constants is only partially successful in eliminating the context-dependent electrostatic contributions from the transferable short-ranged potentials. In particular, Fig. 10b suggests that our initial estimates from the MS-CG potentials systematically under-estimated the effective dielectric constants that are experienced by the sites in the UA simulations.

As described in the Methods section, we employed these transferable short-ranged potentials to obtain more robust estimates for the effective dielectric constants. Figure 8b presents the resulting dielectrics and also the corresponding empirical analytic fit. As expected, these effective dielectrics are larger and also more robust than the dielectrics that we initially estimated from the MS-CG potentials alone, although they demonstrate the same qualitative variation with sulfonation and temperature. The same empirical relation (solid curves) captures these qualitative trends, but provides a poor quantitative fit to the estimated dielectrics. We then employed the transferable short-ranged potentials (Figs. 9)

and 10) with the resulting system-specific dielectric constants (Fig. 8b) to define a single transferable force field for modeling the entire extended ensemble.

Assessment of xn potentials

Figures 11 and 12 characterize the ensembles obtained from simulations with this transferable xn force field. The xn model quite accurately reproduces the UA site-site rdfs at $T=398~\rm K$. In several instances, e.g., the system with 75% sulfonation, the transferable xn model appears more accurate than the MS-CG model specifically parameterized for this system and temperature. Moreover, Fig. 12 demonstrates that the transferable xn force field also reasonably describes the impact of sulfonation upon the effective equilibrium constant for ion-pairing. However, while quite accurate at $T=398~\rm K$, the xn model performs less well at $T=423~\rm K$. In particular, Fig. 12 demonstrates that the xn model does not even qualitatively reproduce the temperature-dependence of the UA rdfs. With increasing temperature, the effective attraction between counter-ions systematically increases in the UA model, while this effective attraction instead decreases or remains unchanged in the xn model.

Accordingly, we inferred that our protocol systematically underestimated the temperature-dependence of the effective dielectrics. Indeed, after we heuristically scaled the dielectrics at T=423 K by a concentration-independent factor of 0.8, the resulting model quite accurately reproduced the high temperature rdfs. Consequently, we adopted a more flexible functional form for the effective dielectric $\epsilon_{\text{eff}} = A(T/T_0)^{-\alpha} \exp{[-bC]}$, while leaving the T=398 K dielectric constants unchanged. The dashed curves in Fig. 8b present this final empirical model for the system-specific dielectric constants. Note that this heuristic rescaling does not impact the dielectrics and, thus, the results for the xn model at T=398 K.

Figure 13 presents the results that are obtained with the xn model at T=423 K after heuristically reducing the effective dielectrics. This scaled extended ensemble (i.e., xn-s) model now reproduces the site-site rdfs of the UA model at T=423 K with reasonable accuracy. More importantly, the dashed blue curve in Fig. 12 demonstrates that, after

heuristically scaling the high-temperature dielectric constants, the xn-s model reasonably reproduces the sensitivity of the ion-pairing equilibrium with respect to variations in both sulfonation and temperature.

Mesoscale charge aggregation with the xn-s model

Since the transferable xn-s model reasonably describes the ion-pairing that is observed in UA simulations, we next employed this model to investigate the temperature-dependence of mesoscale charge aggregation in the fully sulfonated ionomer. Prior experiments ⁶⁹ have demonstrated a characteristic "ionomer peak" at $q=2.5~\rm nm^{-1}$ in the X-ray scattering for the completely sulfonated ionomer. Although its microscopic origin has not been definitively determined, it is generally believed that the ionomer peak reflects a characteristic lengthscale of approximately 2.5 nm between charge aggregates. ⁸⁹ Figure 14a presents the experimentally measured scattering intensity, I(q), for the ionomer peak at $T=353\rm K$, 373K, and 393K, which we have extracted from Figure 1 of Ref. 69. ⁹⁰ Because the experimental scattering was presented in arbitrary units, we have normalized the scattering with respect to the "amorphous halo" feature at $q\approx15~\rm nm^{-1}$. This feature describes the local packing of polymer chains, which is presumably relatively insensitive to temperature. Given this normalization, the ionomer peak of the experimental scattering systematically increases and sharpens as the temperature increases from 353 K to 393 K.

A direct comparison to the experimental scattering is difficult, since the CG model eliminates the vast majority of the atoms that contribute to the experimental scattering. Since the ionomer peak is believed to primarily reflect scattering from charge aggregates, we compare it with the simulated structure factor, S(q), for the ionic sites in the CG model. In calculating the structure factor we have weighted the contribution of each CG site according to the electron density of the corresponding ionic group. Figure 14b presents the structure factor that is calculated from simulations of the fully sulfonated ionomer, while employing the transferable xn-s force field.

At T = 343 K, the simulated structure factor demonstrates a broad peak at q = 5 nm⁻¹ with a shoulder near $q = 3 \text{ nm}^{-1}$. As the temperature increases from T = 343 K to 398 K, the simulated peak grows, sharpens, and gradually shifts to the smaller q characteristic of the ionomer scattering peak. Thus, the CG model appears to demonstrate some features of the mesoscale aggregation that is characterized by the ionomer peak of the experimentally measured scattering. However, in comparison to the experimental ionomer peak at the same temperature, the simulated structure factor is too broad, too small, and peaked at slightly larger q. Interestingly, though, as the temperature is further increased to T=423 K and the effective dielectric constant further reduced to $\epsilon = 3$, the simulated structure factor becomes increasingly reminiscent of the ionomer peak in the experimental scattering intensity. In particular, the simulated structure factor peak becomes increasingly strong, increasingly narrow, and also shifts closer to $q=2.5~\mathrm{nm^{-1}}$. As suggested by the preceding analysis, it appears that our current ad hoc approach does not adequately determine the appropriate system-specific dielectric and, in particular, its temperature-dependence. Nevertheless, the transferable xn-s model appears to capture some of the "physics" governing the ionomer system.

Figure 14c illustrates the string-like aggregates that form in simulations of the xn-s CG model when T=423 K and $\epsilon=3$. This figure presents a 2nm slice through a configuration sampled from simulations in a cubic box with sides of length L=15 nm. The image indicates cation and anion sites by blue and red spheres, respectively, while gray shading indicates connected aggregates. Previous studies have also attributed the ionomer peak to 1-dimensional charge aggregates that form as a consequence of the strong packing constraints that are enforced by the PEO chains linking the sulfonated isophthalate groups. ^{16,89} It is rather remarkable that the exceedingly coarse ionomer model predicts similar aggregates, despite employing only spherically symmetric pair potentials between point sites and eliminating any explicit treatment of the PEO excluded volume.

Discussion

We previously developed a very coarse "ion-only" model for a melt of fully sulfonated PEO-based ionomers at a single temperature. ³² In the present work, we extended this model for 2 different temperatures and 7 different ionomer melts in which varying fractions of the isophthalate groups have been neutralized via hydrolysis. As before, we explicitly represented each diffusing sodium cation and employed a spherical site to represent each isophthalate pendant. By eliminating any explicit representation of the PEO backbone, the CG model provides the necessary efficiency for systematic large scale simulations of mesoscale charge aggregation in glassy ionomers.

We first employed the g-YBG method 77,78,80 to parameterize a distinct MS-CG model 28,71,72 for each ionomer melt at each temperature. These MS-CG models employed soft bond potentials to mimic the connectivity of the PEO backbone and short-ranged pair potentials to describe the effective non-bonded interactions between the sites. The system-specific MS-CG models qualitatively reproduced the "pseudo-bond" distributions sampled by prior UA simulations, including the small coordination peak at short distances and the larger maxima at greater distances, although the MS-CG models tend to sample slightly longer bonds than the UA models. The MS-CG models less accurately reproduced the simulated UA distribution for the ionomer radius of gyration. This effect may be partially due to the slow equilibration of the polymer backbone in the UA simulations. However, it is quite likely that, given this exceedingly coarse representation, the simple approximate potentials cannot adequately describe the conformational statistics of complex ionomers. Indeed, a previous CG model employed a much higher resolution representation in order to accurately describe the conformational properties of polystyrenesulfonate.⁵⁹ More importantly, though, the MS-CG models quite accurately reproduced the ion-pairing that is observed in the UA simulations. In particular, the MS-CG models reproduced the sensitivity of the UA sitesite rdfs to variations in both sulfonation and temperature. Thus, these MS-CG models should provide a reasonable description of ion-pairing in large scale simulations of charge

aggregation in ionomer melts. 32,33

We next employed the extended ensemble framework ⁶⁴ to determine a transferable force field for modeling the entire collection of ionomer melts at both temperatures. We initially attempted to determine a single set of transferable short-ranged potentials for modeling the entire extended ensemble. However, the resulting potentials did not adequately describe the trends in ion-pairing with varying sulfonation or temperature. Consequently, it appears that system-specific Coulomb potentials are necessary to adequately describe the variation of the many-body PMF with temperature and sulfonation. Indeed, several previous studies have demonstrated the importance of system-specific electrostatic potentials for developing transferable CG models of highly charged systems. ^{54–60,62}

In principle, the extended ensemble variational principle may be employed to determine these system-specific dielectrics. However, in this work, we instead determined the dielectrics by fitting the tails of the system-specific MS-CG potentials to Coulomb potentials. The resulting system-specific dielectrics systematically decreased with increasing sulfonation and temperature. In particular, we empirically modeled the dielectrics with an exponential dependence upon the charge density. This simple empirical model quite accurately described the variation in ion-pairing with sulfonation at a single temperature, which is quite consistent with previous studies that modeled the (inverse) dielectric as a linear function of charge concentration. 54,60 In contrast, we found it more challenging to accurately model the temperature-dependence of the effective dielectrics. 58,61,62 In fact, it seems quite likely that our procedure systematically under-estimated the dielectric constants at T=398 K, which necessitated the additional rescaling of the dielectric constants at T=423 K. Clearly, further work is necessary to provide more reliable predictions of the system-specific dielectrics and, especially, their temperature-dependence. This appears quite challenging due to both the complexity of the system and the practical difficulty of determining equilibrium statistics for glassy ionomers.

Nevertheless, despite this rather unsatisfactory treatment of the system-specific dielec-

tric constant, the extended ensemble approach performed reasonably well. First of all, the extended ensemble approach clearly determined a physically reasonable pseudo-bond potential. The calculated transferable bond force function matches quite nicely with the expected force-displacement relation for a freely jointed chain under tension, 87 while employing parameters that closely agree with experimental measurements for the PEO linker. 88 Indeed, the Supplementary Information demonstrates that the transferable xn model provides equivalent accuracy to the MS-CG model for describing the polymer conformations. Secondly, the extended ensemble model quite accurately reproduced the ion-pairing observed in the UA model at T=398 K and also the sensitivity of this ion-pairing to changes in sulfonation. After rescaling the dielectrics at T=423 K, the extended ensemble model reasonably reproduced the rdfs at both temperatures and, moreover, reproduced the variation in ion-pairing with both temperature and sulfonation across the entire extended ensemble.

Moreover, given an appropriate estimate of the system-specific dielectrics, the transferable xn model appears qualitatively consistent with the experimentally observed trends in the ionomer peak of the measured scattering intensity. In particular, the transferable xn-s model predicts the formation of mesoscale charge strings that grow with increasing temperature and sulfonation. ^{32,33} Previous studies have attributed these 1-dimensional ionic aggregates to steric packing constraints generated by the polymer backbone. ^{16,89} It is quite remarkable that the coarse xn model predicts similar 1-dimensional morphologies, since this model does not explicitly describe the steric effects from the polymer backbone and employs spherically symmetric potentials to provide a mean-field description of the effective interactions between sites in the polymer matrix. Thus, it appears that the extended ensemble approach can determine a very low resolution model for ionomers with surprising accuracy and transferability.

These studies also provide additional insight into the balance of physical forces that govern charge conduction in ionomer melts. The MS-CG models demonstrate that the effective interactions between ions become increasingly strong with increasing temperature and sulfonation. Interestingly, in the simple MS-CG models, the ionomers also swell with increasingly strong electrostatic interactions. Finally, the xn model demonstrates the sensitivity of ionic aggregation to slight changes in the effective dielectric. In the initial xn model, increasing temperature results in reduced (or unchanged) ionic aggregation in each ionomer melt. However, reducing the high temperature effective dielectric constant by 20% dramatically reverses this trend in the xn-s model, such that increasing temperature leads to significantly greater charge aggregation for each ionomer, as is observed in the UA simulations. Consequently, the model emphasizes the delicate balance between the entropy loss and the compensating electrostatic energy gain that occur with the growth of ionic aggregates.

Finally, we again emphasize the significant limitations of this work. As noted above, we employed a very ad hoc procedure for modeling the temperature-dependence of the CG potentials. Although the final CG model proved quite successful at two temperatures, the extrapolation to other temperatures is only speculation. Thus, while the extended ensemble approach provides a rigorous framework for developing transferable potentials, further work is clearly necessary to predict or accurately model their temperature-dependence in practice. Moreover, we emphasize that the very coarse ionomer representation limits the predictive capabilities of the model. In particular, the model does not accurately describe the conformations of individual ionomer molecules. More importantly, as a consequence of implicitly modeling the polymer backbone, the current representation cannot directly probe the impact of the backbone upon the structure or dynamics of ion aggregation. Nevertheless, the present results are quite encouraging and strongly motivate further work addressing these limitations.

Conclusion

We employed the extended ensemble framework to develop a transferable force field for very low resolution models of ionomer melts. Our study emphasizes the importance of systemspecific long-ranged electrostatic interactions for achieving reasonable transferability with varying temperature and charge density. In the present work, the system-specific dielectrics systematically decrease with increasing charge density and increasing temperature. The transferable model reasonably reproduces the observed trends in ion-pairing at a particular temperature when the dielectric exponentially varies with sulfonation. In contrast, we find it more challenging to model the temperature-dependence of this dielectric. Nevertheless, given appropriate estimates for the system-specific dielectric constants, the transferable extended ensemble model reasonably reproduces the ion-pairing that is observed in UA simulations of ionomers that range from 25 – 100% sulfonation at two different temperatures. Moreover, the transferable extended ensemble model also qualitatively reproduces the trends in experimental observations of the ionomer peak in the measured scattering intensity. Future work should more carefully consider the temperature-dependence of the effective dielectric and also consider more detailed representations of the PEO backbone that allow for a better description of polymer conformations.

Acknowledgments

JFR acknowledges funding by the Penn State Academic Computing Fellowship. KL acknowledges funding by the Penn State Diefenderfer Graduate Fellowship. JKM acknowledges funding (Grant #0000219054) from the DOE Basic Energy Sciences, Neutron Scattering Program. WGN acknowledges funding (grant Nos. MCB 1053970 and CHE 1565631) from the National Science Foundation in support of this work. Numerical calculations were performed using support and resources from Research Computing and Cyberinfrastructure, a unit of Information Technology Services at Penn State. Figure 1 employed VMD. VMD is developed with NIH support by the Theoretical and Computational Biophysics group at the Beckman Institute, University of Illinois at Urbana-Champaign.

Supporting Information

Further analysis of statistical sampling in the UA simulations, the calculated potentials, as well as the intra-molecular and site-site distributions for each model of each ionomer melt at each temperature. This information is available free of charge via the Internet at http://pubs.acs.org

References

- (1) Schlick, T.; Collepardo-Guevara, R.; Halvorsen, L. A.; Jung, S.; Xiao, X. Biomolecular modeling and simulation: a field coming of age. Quart. Rev. Biophys. 2011, 44, 191– 228.
- (2) Peter, C.; Kremer, K. Multiscale simulation of soft matter systems. Faraday Disc. **2010**, 144, 9–24.
- (3) Eisenberg, A.; Kim, J.-S. *Introduction to Ionomers*; Wiley: New York, 1998.
- (4) Fragiadakis, D.; Dou, S.; Colby, R. H.; Runt, J. Molecular mobility and Li[sup +] conduction in polyester copolymer ionomers based on poly(ethylene oxide). *J. Chem. Phys.* **2009**, *130*, 064907.
- (5) Wang, W.; Liu, W.; Tudryn, G. J.; Colby, R. H.; Winey, K. I. Multi-Length Scale Morphology of Poly(ethylene oxide)-Based Sulfonate Ionomers with Alkali Cations at Room Temperature. *Macromolecules* 2010, 43, 4223–4229.
- (6) Lin, K.-J.; Maranas, J. K. Cation Coordination and Motion in a Poly(ethylene oxide)-Based Single Ion Conductor. *Macromolecules* **2012**, *45*, 6230–6240.
- (7) Maranas, J. K. Polymers for Energy Storage and Delivery: Polyelectrolytes for Batteries and Fuel Cells; 2012; Chapter 2, pp 1–17.
- (8) Klein, M. L.; Shinoda, W. Large-scale molecular dynamics simulations of self-assembling systems. *Science* **2008**, *321*, 798–800.
- (9) Müller, M.; de Pablo, J. J. Computational Approaches for the Dynamics of Structure Formation in Self-Assembling Polymeric Materials. *Annu. Rev. Mat. Res.* **2013**, *43*, 1–34.
- (10) Noid, W. G. Perspective: Coarse-grained models for biomolecular systems. *J. Chem. Phys.* **2013**, *139*, 090901.

- (11) Muller, M.; Katsov, K.; Schick, M. Biological and synthetic membranes: What can be learned from a coarse-grained description? *Phys. Rep.* **2006**, *434*, 113–176.
- (12) Schmid, F. Toy amphiphiles on the computer: What can we learn from generic models? Macromol. Rapid Comm. 2009, 30, 741–751.
- (13) Hyeon, C.; Thirumalai, D. Capturing the essence of folding and functions of biomolecules using coarse-grained models. *Nat. Commun.* **2011**, *2*, 487.
- (14) Goswami, M.; Kumar, S. K.; Bhattacharya, A.; Douglas, J. F. Computer Simulations of Ionomer Self-Assembly and Dynamics. *Macromolecules* **2007**, *40*, 4113–4118.
- (15) Hall, L. M.; Stevens, M. J.; Frischknecht, A. L. Effect of Polymer Architecture and Ionic Aggregation on the Scattering Peak in Model Ionomers. *Phys. Rev. Lett.* 2011, 106, 127801.
- (16) Hall, L. M.; Seitz, M. E.; Winey, K. I.; Opper, K. L.; Wagener, K. B.; Stevens, M. J.; Frischknecht, A. L. Ionic Aggregate Structure in Ionomer Melts: Effect of Molecular Architecture on Aggregates and the Ionomer Peak. J. Am. Chem. Soc. 2012, 134, 574–587.
- (17) Hall, L. M.; Stevens, M. J.; Frischknecht, A. L. Dynamics of Model Ionomer Melts of Various Architectures. *Macromolecules* **2012**, *45*, 8097–8108.
- (18) Murtola, T.; Bunker, A.; Vattulainen, I.; Deserno, M.; Karttunen, M. Multiscale modeling of emergent materials: Biological and soft matter. *Phys. Chem. Chem. Phys.* 2009, 11, 1869–92.
- (19) Brini, E.; Algaer, E. A.; Ganguly, P.; Li, C.; Rodriguez-Ropero, F.; van der Vegt, N. F. A. Systematic coarse-graining methods for soft matter simulations a review. Soft Matter 2013, 9, 2108–2119.

- (20) Saunders, M. G.; Voth, G. A. Coarse-Graining Methods for Computational Biology.

 Annu. Rev. Biophys. 2013, 42, 73–93.
- (21) Noid, W. G. Systematic methods for structurally consistent coarse-grained models.

 Methods Mol Biol 2013, 924, 487–531.
- (22) Wagner, J. W.; Dama, J. F.; Durumeric, A. E. P.; Voth, G. A. On the representability problem and the physical meaning of coarse-grained models. *The Journal of Chemical Physics* **2016**, *145*, 044108.
- (23) Dunn, N. J. H.; Foley, T. T.; Noid, W. G. Van der Waals Perspective on Coarse-Graining: Progress toward Solving Representability and Transferability Problems. *Acc. Chem. Res.* **2016**, *49*, 2832–2840.
- (24) Kirkwood, J. G. Statistical mechanics of fluid mixtures. *J. Chem. Phys.* **1935**, *3*, 300–313.
- (25) Liwo, A.; Oldziej, S.; Pincus, M. R.; Wawak, R. J.; Rackovsky, S.; Scheraga, H. A. A united-residue force field for off-lattice protein-structure simulations. 1. Functional forms and parameters of long-range side-chain interaction potentials from protein crystal data. J. Comp. Chem. 1997, 18, 849–73.
- (26) Likos, C. N. Effective interactions in soft condensed matter physics. *Phys. Rep.* **2001**, 348, 267 439.
- (27) Akkermans, R. L. C.; Briels, W. J. A structure-based coarse-grained model for polymer melts. J. Chem. Phys. **2001**, 114, 1020–1031.
- (28) Noid, W. G.; Chu, J.-W.; Ayton, G. S.; Krishna, V.; Izvekov, S.; Voth, G. A.; Das, A.; Andersen, H. C. The Multiscale Coarse-graining Method. I. A Rigorous Bridge between Atomistic and Coarse-grained Models. J. Chem. Phys. 2008, 128, 244114.

- (29) Lyubartsev, A. P.; Laaksonen, A. Calculation of effective interaction potentials from radial distribution functions: A reverse Monte Carlo approach. *Phys. Rev. E* **1995**, *52*, 3730–37.
- (30) Müller-Plathe, F. Coarse-graining in polymer simulation: From the atomistic to the mesoscopic scale and back. *ChemPhysChem* **2002**, *3*, 754 769.
- (31) Shell, M. S. The relative entropy is fundamental to multiscale and inverse thermodynamic problems. *J. Chem. Phys.* **2008**, *129*, 144108.
- (32) Lu, K.; Rudzinski, J. F.; Noid, W. G.; Milner, S. T.; Maranas, J. K. Scaling behavior and local structure of ion aggregates in single-ion conductors. *Soft Matter* **2014**, *10*, 978–989.
- (33) Lu, K.; Maranas, J. K.; Milner, S. T. Ion-mediated charge transport in ionomeric electrolytes. *Soft Matter* **2016**, *12*, 3943–3954.
- (34) Chen, Q.; Tudryn, G. J.; Colby, R. H. Ionomer dynamics and the sticky Rouse model.

 J. Rheol. (N. Y. N. Y). 2013, 57, 1441.
- (35) Lin, K.-J.; Maranas, J. K. Superionic behavior in polyethylene-oxidebased single-ion conductors. *Phys. Rev. E* **2013**, *88*, 052602.
- (36) Louis, A. A.; Bolhuis, P. G.; Hansen, J. P.; Meijer, E. J. Can polymer coils be modeled as "soft colloids". *Phys. Rev. Lett.* **2000**, *85*, 2522–5.
- (37) Vettorel, T.; Meyer, H. Coarse graining of short polyethylene chains for studying polymer crystallization. J. Chem. Theor. Comp. 2006, 2, 616–629.
- (38) Ghosh, J.; Faller, R. State point dependence of systematically coarse-grained potentials.

 Mol. Sim. 2007, 33, 759–767.
- (39) Johnson, M. E.; Head-Gordon, T.; Louis, A. A. Representability problems for coarse-grained water potentials. *J. Chem. Phys.* **2007**, *126*, 144509.

- (40) Allen, E. C.; Rutledge, G. C. A novel algorithm for creating coarse-grained, density dependent implicit solvent models. *J. Chem. Phys.* **2008**, *128*, 154115.
- (41) Krishna, V.; Noid, W. G.; Voth, G. A. The multiscale coarse-graining method. IV. Transferring coarse-grained potentials between temperatures. J. Chem. Phys. 2009, 131, 024103.
- (42) Chaimovich, A.; Shell, M. S. Anomalous waterlike behavior in spherically-symmetric water models optimized with the relative entropy. *Phys. Chem. Chem. Phys.* **2009**, *11*, 1901–1915.
- (43) Lu, L.; Voth, G. A. The multiscale coarse-graining method. VII. Free energy decomposition of coarse-grained effective potentials. *J. Chem. Phys.* **2011**, *134*, 224107.
- (44) Izvekov, S. Towards an understanding of many-particle effects in hydrophobic association in methane solutions. *J. Chem. Phys.* **2011**, *134*, 034104.
- (45) Farah, K.; Fogarty, A. C.; Böhm, M. C.; Müller-Plathe, F. Temperature dependence of coarse-grained potentials for liquid hexane. *Phys. Chem. Chem. Phys.* **2011**, *13*, 2894–902.
- (46) McCarty, J.; Clark, A. J.; Copperman, J.; Guenza, M. G. An analytical coarse-graining method which preserves the free energy, structural correlations, and thermodynamic state of polymer melts from the atomistic to the mesoscale. *J. Chem. Phys.* **2014**, *140*.
- (47) Hills, R. D.; Lu, L. Y.; Voth, G. A. Multiscale Coarse-Graining of the Protein Energy Landscape. *PLoS Comput. Biol.* **2010**, *6*, e1000827.
- (48) Thorpe, I. F.; Goldenberg, D. P.; Voth, G. A. Exploration of transferability in multiscale coarse-grained peptide models. *J. Phys. Chem. B* **2011**, *115*, 11911–26.
- (49) Engin, O.; Villa, A.; Peter, C.; Sayar, M. A Challenge for Peptide Coarse Graining: Transferability of Fragment-Based Models. *Macromol. Theory Sim.* **2011**, *20*, 451–465.

- (50) Dalgicdir, C.; Sensoy, O.; Peter, C.; Sayar, M. A transferable coarse-grained model for diphenylalanine: How to represent an environment driven conformational transition. J. Chem. Phys. 2013, 139.
- (51) Moore, T. C.; Iacovella, C. R.; McCabe, C. Derivation of coarse-grained potentials via multistate iterative Boltzmann inversion. *J. Chem. Phys.* **2014**, *140*.
- (52) Zhang, J.; Guo, H. Transferability of Coarse-Grained Force Field for nCB Liquid Crystal Systems. J. Phys. Chem. B 2014, 118, 4647–4660.
- (53) Bereau, T.; Wang, Z.-J.; Deserno, M. More than the sum of its parts: Coarse-grained peptide-lipid interactions from a simple cross-parametrization. *J. Chem. Phys.* **2014**, 140.
- (54) Hess, B.; Holm, C.; van der Vegt, N. Modeling Multibody Effects in Ionic Solutions with a Concentration Dependent Dielectric Permittivity. Phys. Rev. Lett. 2006, 96, 147801.
- (55) Lyubartsev, A. P.; Laaksonen, A. Osmotic and activity coefficients from effective potentials for hydrated ions. *Phys. Rev. E* **1997**, *55*, 5689–5696.
- (56) Savelyev, A.; Papoian, G. A. Molecular renormalization group coarse-graining of electrolyte solutions: Applications to aqueous NaCl and KCl. J. Phys. Chem. B 2009, 113, 7785–93.
- (57) Kalcher, I.; Dzubiella, J. Structure-thermodynamics relation of electrolyte solutions. *J. Chem. Phys.* **2009**, *130*.
- (58) Mirzoev, A.; Lyubartsev, A. P. Effective solvent mediated potentials of Na+ and Clions in aqueous solution: temperature dependence. Phys. Chem. Chem. Phys. 2011, 13, 5722–5727.

- (59) Li, C.; Shen, J.; Peter, C.; van der Vegt, N. F. A. A Chemically Accurate Implicit-Solvent Coarse-Grained Model for Polystyrenesulfonate Solutions. *Macromolecules* **2012**, 45, 2551–2561.
- (60) Shen, J.-W.; Li, C.; van der Vegt, N. F.; Peter, C. Transferability of Coarse Grained Potentials: Implicit Solvent Models for Hydrated Ions. J. Chem. Theor. Comp. 2011, 7, 1916–1927.
- (61) Cao, Z.; Dama, J. F.; Lu, L.; Voth, G. A. Solvent Free Ionic Solution Models from Multiscale Coarse-Graining. J. Chem. Theor. Comp. 2013, 9, 172–178.
- (62) Wang, Y. T.; Izvekov, S.; Yan, T. Y.; Voth, G. A. Multiscale coarse-graining of ionic liquids. J. Phys. Chem. B 2006, 110, 3564 3575.
- (63) Foley, T. T.; Shell, M. S.; Noid, W. G. The impact of resolution upon entropy and information in coarse-grained models. *J. Chem. Phys.* **2015**, *143*, 243104.
- (64) Mullinax, J. W.; Noid, W. G. Extended Ensemble approach for deriving transferable Coarse-grained potentials. *J. Chem. Phys.* **2009**, *131*, 104110.
- (65) Mullinax, J. W.; Noid, W. G. Recovering physical potentials from a model protein databank. *Proc. Natl. Acad. Sci. USA* **2010**, *107*, 19867–72.
- (66) Dunn, N. J. H.; Noid, W. G. Bottom-up coarse-grained models with predictive accuracy and transferability for both structural and thermodynamic properties of heptane-toluene mixtures. J. Chem. Phys. 2016, 144, 204124.
- (67) Sinha, K.; Maranas, J. K. Segmental Dynamics and Ion Association in PEO-Based Single Ion Conductors. *Macromolecules* 2011, 44, 5381–5391.
- (68) Caldwell II, D. W.; Maranas, J. K. Manuscript in preparation.

- (69) Wang, W.; Tudryn, G. J.; Colby, R. H.; Winey, K. I. Thermally Driven Ionic Aggregation in Poly(ethylene oxide)-Based Sulfonate Ionomers. J. Am. Chem. Soc. 2011, 133, 10826–10831.
- (70) Ercolessi, F.; Adams, J. B. Interatomic potentials from first-principles calculations: The force-matching method. *Europhys. Lett.* **1994**, *26*, 583.
- (71) Izvekov, S.; Voth, G. A. A multiscale coarse-graining method for biomolecular systems.

 J. Phys. Chem. B 2005, 109, 2469 2473.
- (72) Izvekov, S.; Voth, G. A. Multiscale coarse graining of liquid-state systems. *J. Chem. Phys.* **2005**, *123*, 134105.
- (73) Noid, W. G.; Liu, P.; Wang, Y. T.; Chu, J.-W.; Ayton, G. S.; Izvekov, S.; Andersen, H. C.; Voth, G. A. The Multiscale Coarse-graining Method. II. Numerical implementation for molecular coarse-grained models. *J. Chem. Phys.* **2008**, *128*, 244115.
- (74) Lu, L. Y.; Izvekov, S.; Das, A.; Andersen, H. C.; Voth, G. A. Efficient, Regularized, and Scalable Algorithms for Multiscale Coarse-Graining. *J. Chem. Theor. Comp.* **2010**, *6*, 954–965.
- (75) Mullinax, J. W.; Noid, W. G. Reference state for the generalized Yvon-Born-Green theory: Application for a coarse-grained model of hydrophobic hydration. J. Chem. Phys. 2010, 133, 124107.
- (76) Noid, W. G.; Chu, J.-W.; Ayton, G. S.; Voth, G. A. Multiscale Coarse-graining and Structural Correlations: Connections to Liquid State Theory. *J. Phys. Chem. B* **2007**, 111, 4116–27.
- (77) Mullinax, J. W.; Noid, W. G. A Generalized Yvon-Born-Green Theory for Determining Coarse-grained Interaction Potentials. *J. Phys. Chem. C* **2010**, *114*, 5661–74.

- (78) Rudzinski, J. F.; Noid, W. G. A generalized-Yvon-Born-Green method for coarse-grained modeling. *Eur. Phys. J. ST* **2015**, *224*, 2193–2216.
- (79) Ruhle, V.; Junghans, C.; Lukyanov, A.; Kremer, K.; Andrienko, D. Versatile Object-Oriented Toolkit for Coarse-Graining Applications. *J. Chem. Theor. Comp.* **2009**, *5*, 3211–3223.
- (80) Mullinax, J. W.; Noid, W. G. A generalized Yvon-Born-Green theory for molecular systems. *Phys. Rev. Lett.* **2009**, *103*, 198104.
- (81) Rudzinski, J. F.; Noid, W. G. Investigation of Coarse-Grained Mappings via an Iterative Generalized Yvon-Born-Green Method. J. Phys. Chem. B 2014, 118, 8295–8312.
- (82) Hess, B.; Kutzner, C.; van der Spoel, D.; Lindahl, E. GROMACS 4: Algorithms for Highly Efficient, Load-Balanced, and Scalable Molecular Simulation. J. Chem. Theor. Comp. 2008, 4, 435–447.
- (83) Kremer, F.; Schonhals, A. In *Broadband Dielectric Spectroscopy*; Kremer, F., Schönhals, A., Eds.; Springer Berlin Heidelberg: Berlin, Heidelberg, 2003.
- (84) Bussi, G.; Donadio, D.; Parrinello, M. Canonical sampling through velocity rescaling.
 J. Chem. Phys. 2007, 126, 014101.
- (85) Darden, T.; York, D.; Pedersen, L. Particle mesh Ewald: An N log(N) method for Ewald sums in large systems. J. Chem. Phys. 1993, 98, 10089–10092.
- (86) Gilson, M. K.; Given, J. A.; Bush, B. L.; McCammon, J. A. The statistical-thermodynamic basis for computation of binding affinities: a critical review. *Biophys. J.* 1997, 72, 1047–1069.
- (87) Rubinstein, M.; Colby, R. Polymer Physics; Oxford University Press: New York, 2003.

- (88) Fetters, L. J.; Lohse, D. J.; Richter, D.; Witten, T. A.; Zirkel, A. Connection between Polymer Molecular Weight, Density, Chain Dimensions, and Melt Viscoelastic Properties. *Macromolecules* **1994**, *27*, 4639–4647.
- (89) Buitrago, C. F.; Bolintineanu, D. S.; Seitz, M. E.; Opper, K. L.; Wagener, K. B.; Stevens, M. J.; Frischknecht, A. L.; Winey, K. I. Direct Comparisons of X-ray Scattering and Atomistic Molecular Dynamics Simulations for Precise Acid Copolymers and Ionomers. *Macromolecules* 2015, 48, 1210–1220.
- (90) We extracted the data from the published PDF figure with GraphClick from Arizona Software. Accessed 6/13/2016. Available at http://www.arizona-software.ch/graphclick/.

Tables

Table 1: Ionomer melts simulated with CG models at $T=398~\mathrm{K}$ and 423 K. L indicates the length (in units of nm) of the sides for the cubic supercells employed for parameterizing the CG models and for subsequent CG simulations at the two temperatures. N and N_{Na} indicate the number of CG sites and Na sites, respectively, employed in the CG representations of each melt.

% Sulfonation	$L_{398\mathrm{K}}$	L_{423K}	N	$N_{ m Na}$
25	14.63	14.50	3645	729
38	14.69	14.72	4023	1107
50	14.73	14.78	4374	1458
63	14.69	14.82	4752	1836
75	14.76	14.82	5103	2187
83	14.77	14.86	5346	2430
100	14.76	14.88	5832	2916

Figure Captions

- Figure 1 Simulated PEO-based ionomers. The top image describes the chemical structure of the simulated ionomers. For ionomer systems with incomplete sulfonation, i.e., $x \leq 1$, the neutralized isophthalate sites are randomly distributed among the ionomers. (The previously published ion-only CG model corresponds to $x=1.^{32}$) The middle image superimposes the CG representation upon the chemical structure: the red, blue, and green circles indicate the S, Na, and C sites that are explicitly represented in the CG model. The bottom image represents the conformation of a single ionomer chain that has been sampled from previous UA simulations of the melt. This image highlights the isophthalate groups in orange, while the carbon and ether oxygen atoms of the PEO linker are indicated by cyan and red, respectively. The large green, red, and blue spheres indicate C, S, and Na sites, respectively, in the mapped CG representation of the conformation.
- Figure 2 Equilibration of ion-pairing statistics as quantified by $P_2(\tau)$ for UA simulation at $T=398 \mathrm{K}$ (top) and 423K (bottom). The blue, cyan, magenta, and red curves present $P_2(\tau)$ for ionomer melts with 25, 50, 75, and 100% sulfonation, respectively. The horizontal dashed lines indicate the expected long-time asymptotes for the ion-pairing statistics, i.e., $P_{\infty} \equiv 2P_2(0)^2/N$ for each simulation. The colored vertical bands indicate the time scales for which $P_2(\tau)$ is characterized by exponential decay, power law decay, and random fluctuations, which correspond, respectively, to initial dissociation, correlated diffusion, and uncorrelated diffusion of the cations.
- Figure 3 Calculated bond potentials for the system-specific MS-CG models. The top and bottom rows correspond to $T=398\mathrm{K}$ and $T=423\mathrm{K}$, respectively. In each row, the smaller right panel highlights the contact minima of the bond potentials. The blue, cyan, magenta, and red curves present results for ionomer melts with 25, 50, 75, and 100% sulfonation, respectively. Potentials are presented in units of kJ/mol.

- Figure 4 Calculated nonbonded pair potentials for the system-specific MS-CG models at $T=398 \mathrm{K}$. Rows (i), (ii), and (iii) present the C-C, S-Na, and S-S pair potentials, respectively. In each row, the smaller right panel highlights the minimum of the corresponding potential. In the right panel, the solid and dashed curves present the potentials at $T=398 \mathrm{K}$ and 423 K, repectively. The blue, cyan, magenta, and red curves present results for ionomer melts with 25, 50, 75, and 100% sulfonation, respectively. Potentials are presented in units of kJ/mol.
- Figure 5 Comparison of polymer conformations in the UA (solid curves) and system-specific MS-CG models (dashed curves). Rows (i) and (ii) present results for $T=398\mathrm{K}$ and 423K, respectively. Columns (a) and (b) present distributions for the coarse-grained bond length, r_b , and radius of gyration, R_g , respectively. The horizontal lines in column (a) indicate the baselines for the various bond distributions, which have been shifted for clarity, while the vertical lines indicate the maxima of the distributions. The blue, cyan, magenta, and red curves present results for ionomer melts with 25, 50, 75, and 100% sulfonation, respectively.
- Figure 6 Comparison of simulated site-site rdfs in the UA (solid curves) and system-specific MS-CG models (dashed curves). Rows (i) and (ii) present the S-Na and S-S rdfs, respectively, which have been vertically shifted for clarity. In these two rows, the columns (a) and (b) present results for $T=398\mathrm{K}$ and 423K, respectively. The blue, cyan, magenta, and red curves present results for ionomer melts with 25, 50, 75, and 100% sulfonation, respectively.
- Figure 7 Equilibrium constant for charge aggregation in the UA (black curves) and MS-CG (red curves) models as quantified by the area of the first peak in the S-Na rdf, I = $\int dr \, 4\pi r^2 g_{S-Na}(r)$ as a function of sulfonation, %S. The solid and dashed curves correspond to $T=398 {\rm K}$ and 423 K, respectively.
- Figure 8 System-specific dielectrics, $\epsilon_{\Gamma\beta}$. Panel (a) presents the dielectrics initially estimated

by fitting the long-range tail of system-specific MS-CG potentials. Panel (b) presents the dielectrics estimated from the MS-CG potentials after subtracting the transferable short-ranged pair potentials. In both panels, the solid curves indicate the global empirical fit to this data: $\epsilon_{\rm eff} = A(T/T_0)^{-1} \exp\left[-bC\right]$. The dashed curves in panel (b) present the final empirical fit to system-specific dielectrics: $\epsilon_{\rm eff} = A(T/T_0)^{-\alpha} \exp\left[-bC\right]$. Blue, cyan, magenta, and red indicate results for ionomer melts with 25, 50, 75, and 100% sulfonation, respectively.

- Figure 9 Panel (a) presents the calculated transferable bond potential, $U_b(r_b)$. Panel (b) compares the corresponding tension $F_b = +dU_b/dr_b$ (crosses) with the shifted Langevin curve for the average length of a freely jointed chain under equivalent tension (solid curve).
- Figure 10 Calculated transferable xn non-bonded short-ranged pair potentials. Potentials are presented in units of kJ/mol.
- Figure 11 Comparison of simulated site-site rdfs in in the UA (solid curves) and in the initial transferable xn (dashed curves) models. Rows (i) and (ii) present the S-Na and S-S rdfs, respectively. In these two rows, the columns (a) and (b) present results for $T=398\mathrm{K}$ and 423K, respectively. The blue, cyan, magenta, and red curves present results for ionomer melts with 25, 50, 75, and 100% sulfonation, respectively
- Figure 12 Equilibrium constant for charge aggregation as quantified by the area of the first peak in the S-Na rdf, $I = \int dr \, 4\pi r^2 g_{S-Na}(r)$ as a function of sulfonation, %S. The black and red curves correspond to the UA and to the initial xn models, respectively, while the solid and dashed curves correspond to T = 398K and 423K, respectively. The dashed blue curve presents results for the final xn model at T = 423 K after heuristically rescaling the dielectric at this temperature.
- Figure 13 Comparison of simulated site-site rdfs at $T=423\mathrm{K}$ in the UA model (solid curves) and

in the final transferable xn model (dashed curves) after rescaling the system-specific dielectrics at T=423K. Rows (i) and (ii) present simulated rdfs for the S-Na and S-S site pairs, respectively. The blue, cyan, magenta, and red curves present results for ionomer melts with 25, 50, 75, and 100% sulfonation, respectively.

Figure 14 Comparison of experiments and simulations characterizing the temperature dependence of charge aggregation in the fully sulfonated ionomer melt. Panel (a) presents the ionomer feature in the measured X-ray scattering data extracted from Figure 1 of Ref. 69 after rescaling with respect to the "amorphous halo" feature at $q \approx 15 \text{ nm}^{-1}$. Panel (b) presents the structure factor calculated from simulations of the fully sulfonated ionomer with the xn-s force field. The orange and purple curves in panel (b) are calculated from CG simulations at 423K in which the dielectric constant has been further reduced to the values denoted in the legend. The bottom panel indicates the aggregation of cations (blue) and anions (red) in a simulated configuration of the fully sulfonated ionomer melt with the xn model at T = 423 K after further reducing the dielectric to $\epsilon = 3$. The image indicates the ions within a 2 nm slice through a cubic simulation box with sides of length L = 15 nm, while the background provides a grid with 1 nm resolution in the x- and y- directions.

Figures

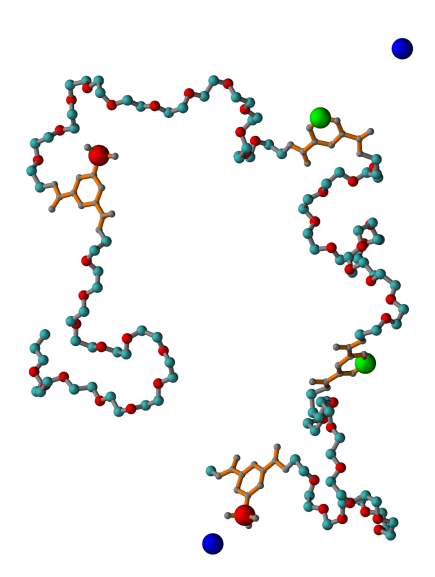


Figure 1: Simulated PEO-based ionomers. The top image describes the chemical structure of the simulated ionomers. For ionomer systems with incomplete sulfonation, i.e., $x \leq 1$, the neutralized isophthalate sites are randomly distributed among the ionomers. (The previously published ion-only CG model corresponds to $x=1.^{32}$) The middle image superimposes the CG representation upon the chemical structure: the red, blue, and green circles indicate the S, Na, and C sites that are explicitly represented in the CG model. The bottom image represents the conformation of a single ionomer chain that has been sampled from previous UA simulations of the melt. This image highlights the isophthalate groups in orange, while the carbon and ether oxygen atoms of the PEO linker are indicated by cyan and red, respectively. The large green, red, and blue spheres indicate C, S, and Na sites, respectively, in the mapped CG representation of the conformation.

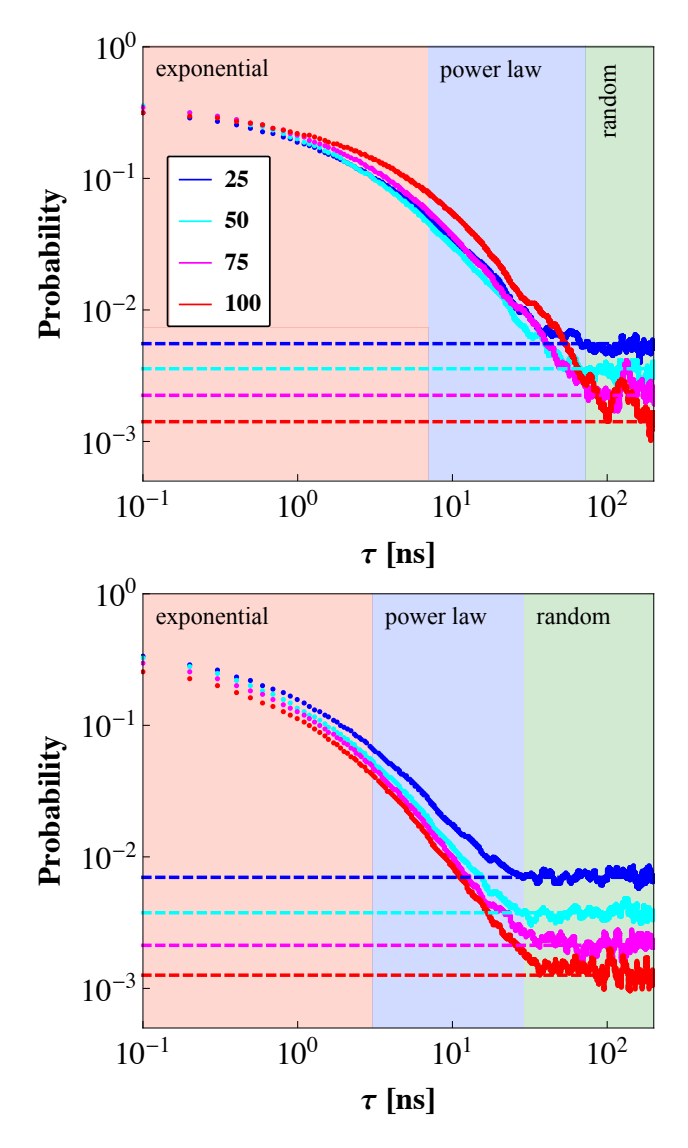


Figure 2: Equilibration of ion-pairing statistics as quantified by $P_2(\tau)$ for UA simulation at $T=398 \mathrm{K}$ (top) and 423K (bottom). The blue, cyan, magenta, and red curves present $P_2(\tau)$ for ionomer melts with 25, 50, 75, and 100% sulfonation, respectively. The horizontal dashed lines indicate the expected long-time asymptotes for the ion-pairing statistics, i.e., $P_{\infty} \equiv 2P_2(0)^2/N$ for each simulation. The colored vertical bands indicate the time scales for which $P_2(\tau)$ is characterized by exponential decay, power law decay, and random fluctuations, which correspond, respectively, to initial dissociation, correlated diffusion, and uncorrelated diffusion of the cations.

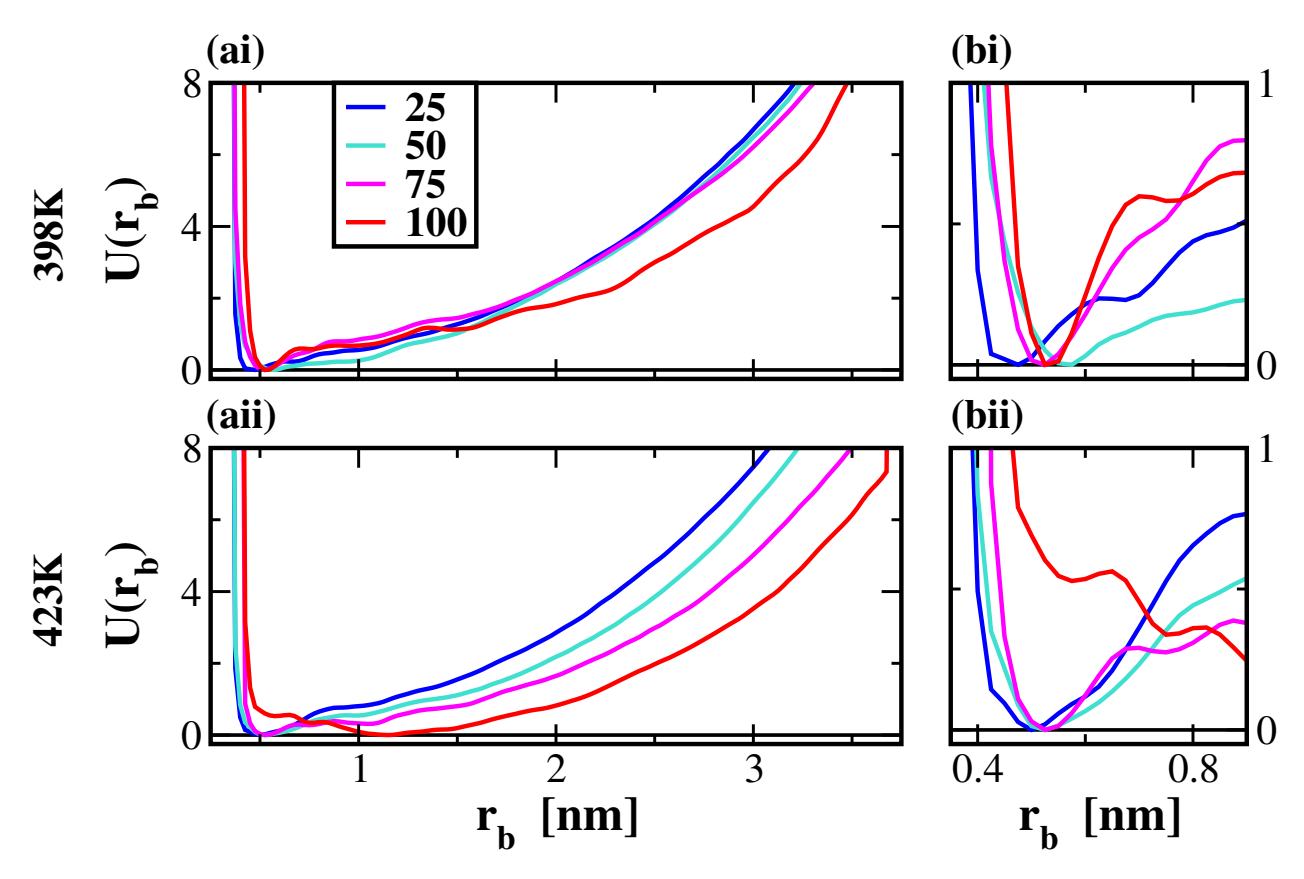


Figure 3: Calculated bond potentials for the system-specific MS-CG models. The top and bottom rows correspond to $T=398\mathrm{K}$ and $T=423\mathrm{K}$, respectively. In each row, the smaller right panel highlights the contact minima of the bond potentials. The blue, cyan, magenta, and red curves present results for ionomer melts with 25, 50, 75, and 100% sulfonation, respectively. Potentials are presented in units of kJ/mol.

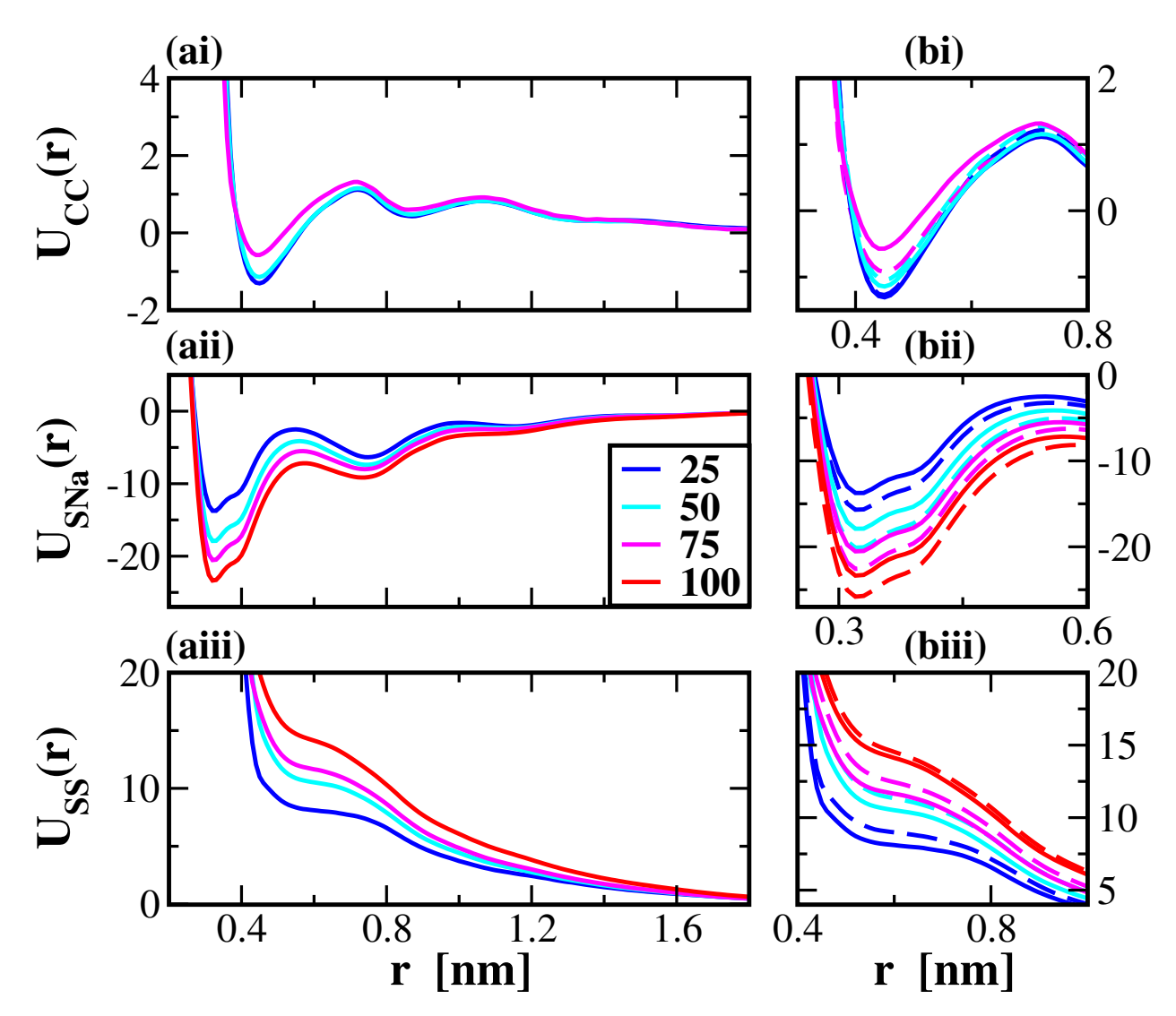


Figure 4: Calculated nonbonded pair potentials for the system-specific MS-CG models at $T=398\mathrm{K}$. Rows (i), (ii), and (iii) present the C-C, S-Na, and S-S pair potentials, respectively. In each row, the smaller right panel highlights the minimum of the corresponding potential. In the right panel, the solid and dashed curves present the potentials at $T=398\mathrm{K}$ and 423K, repectively. The blue, cyan, magenta, and red curves present results for ionomer melts with 25, 50, 75, and 100% sulfonation, respectively. Potentials are presented in units of kJ/mol.

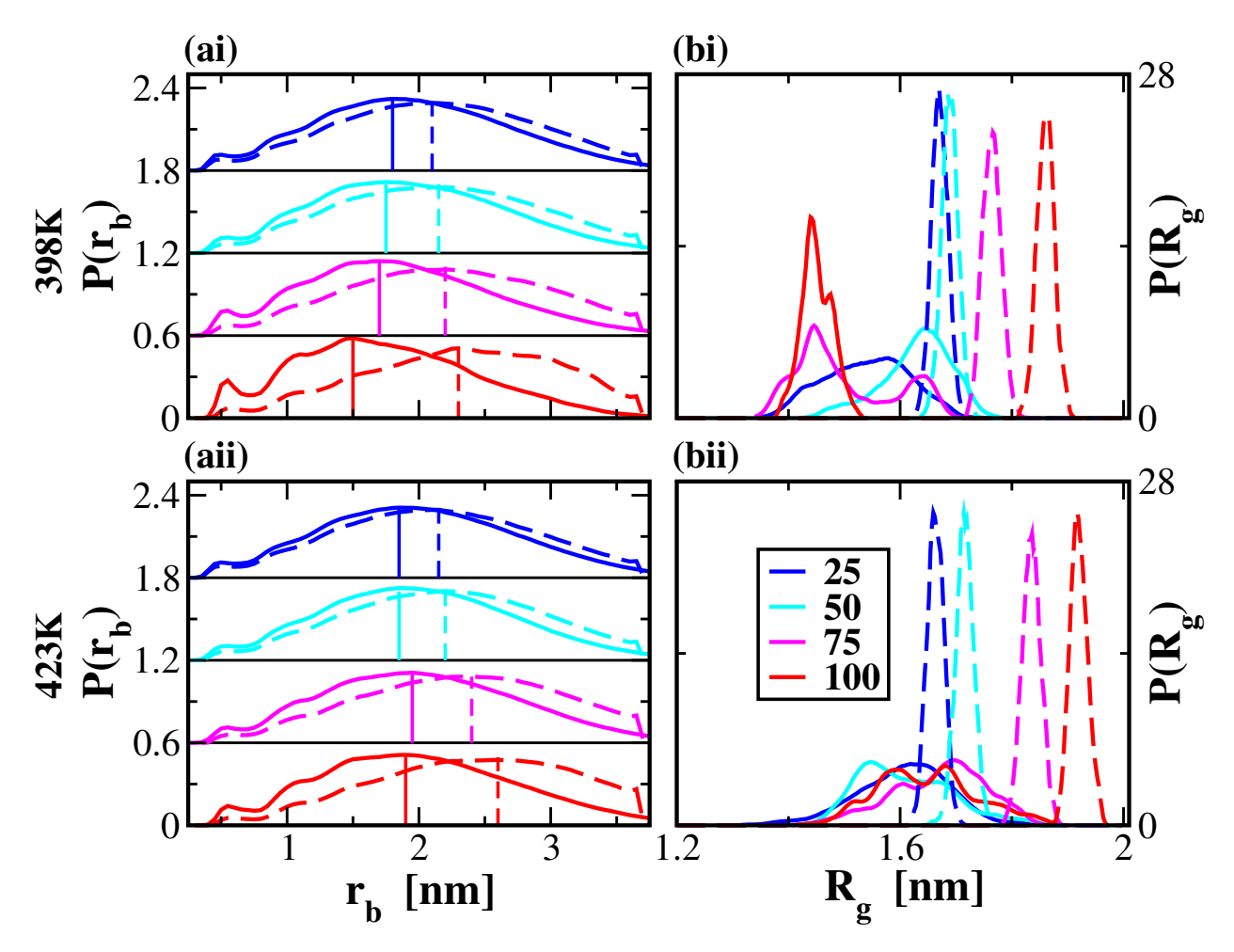


Figure 5: Comparison of polymer conformations in the UA (solid curves) and system-specific MS-CG models (dashed curves). Rows (i) and (ii) present results for $T=398\mathrm{K}$ and 423K, respectively. Columns (a) and (b) present distributions for the coarse-grained bond length, $r_{\rm b}$, and radius of gyration, $R_{\rm g}$, respectively. The horizontal lines in column (a) indicate the baselines for the various bond distributions, which have been shifted for clarity, while the vertical lines indicate the maxima of the distributions. The blue, cyan, magenta, and red curves present results for ionomer melts with 25, 50, 75, and 100% sulfonation, respectively.

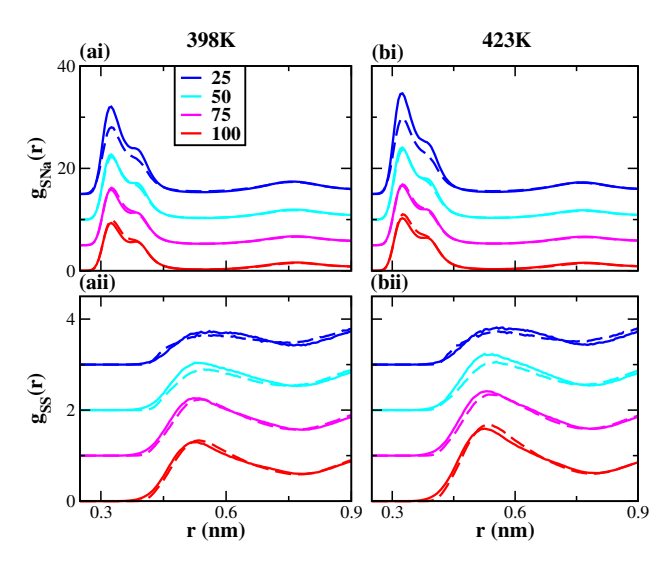


Figure 6: Comparison of simulated site-site rdfs in the UA (solid curves) and system-specific MS-CG models (dashed curves). Rows (i) and (ii) present the S-Na and S-S rdfs, respectively, which have been vertically shifted for clarity. In these two rows, the columns (a) and (b) present results for $T=398\mathrm{K}$ and $423\mathrm{K}$, respectively. The blue, cyan, magenta, and red curves present results for ionomer melts with 25, 50, 75, and 100% sulfonation, respectively.

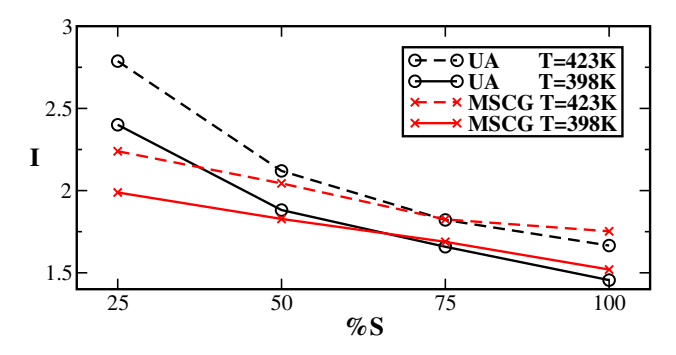


Figure 7: Equilibrium constant for charge aggregation in the UA (black curves) and MS-CG (red curves) models as quantified by the area of the first peak in the S-Na rdf, I = $\int dr \, 4\pi r^2 g_{\rm S-Na}(r)$ as a function of sulfonation, %S. The solid and dashed curves correspond to $T=398{\rm K}$ and 423K, respectively.

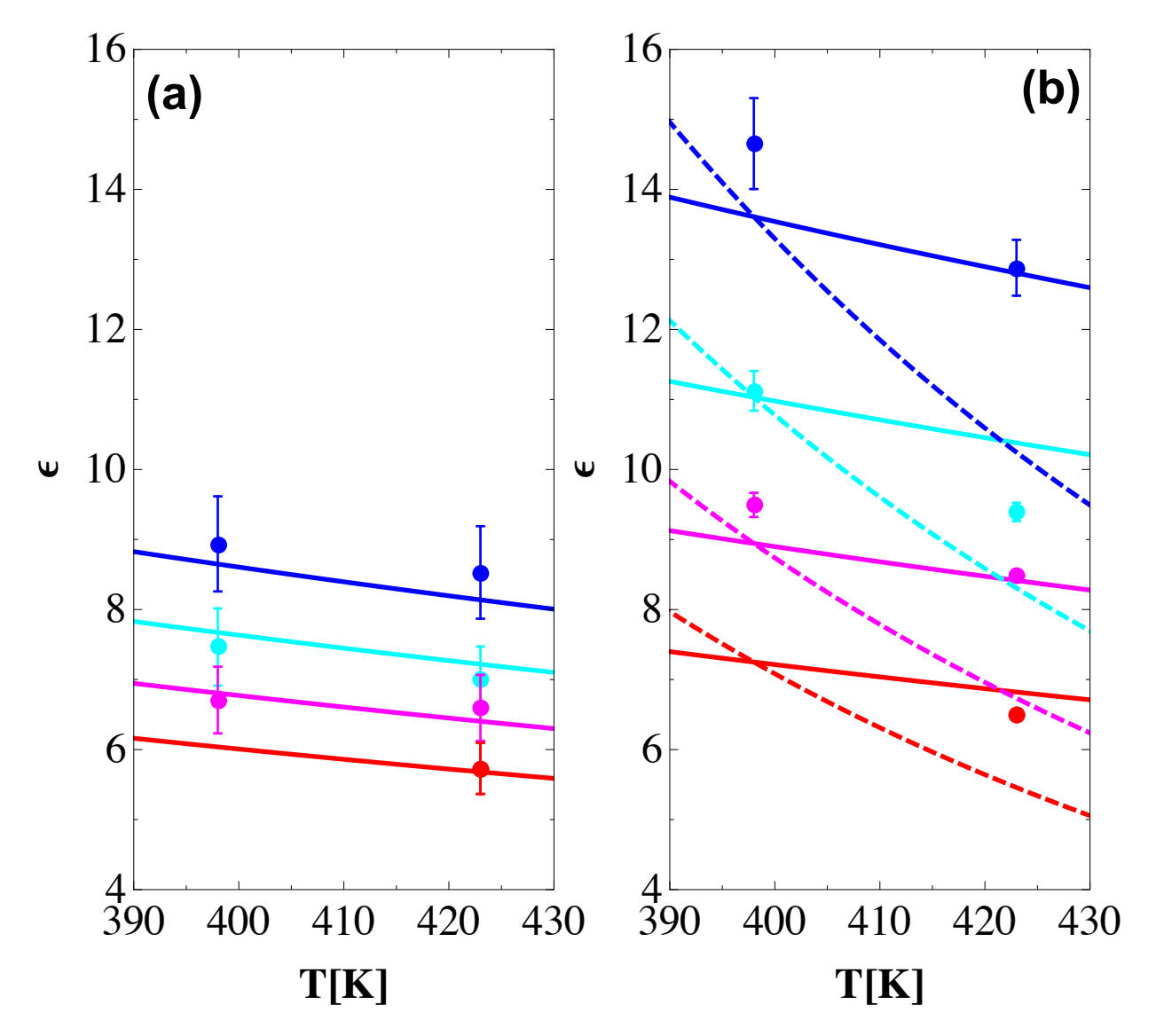


Figure 8: System-specific dielectrics, $\epsilon_{\Gamma\beta}$. Panel (a) presents the dielectrics initially estimated by fitting the long-range tail of system-specific MS-CG potentials. Panel (b) presents the dielectrics estimated from the MS-CG potentials after subtracting the transferable short-ranged pair potentials. In both panels, the solid curves indicate the global empirical fit to this data: $\epsilon_{\text{eff}} = A(T/T_0)^{-1} \exp\left[-bC\right]$. The dashed curves in panel (b) present the final empirical fit to system-specific dielectrics: $\epsilon_{\text{eff}} = A(T/T_0)^{-\alpha} \exp\left[-bC\right]$. Blue, cyan, magenta, and red indicate results for ionomer melts with 25, 50, 75, and 100% sulfonation, respectively.

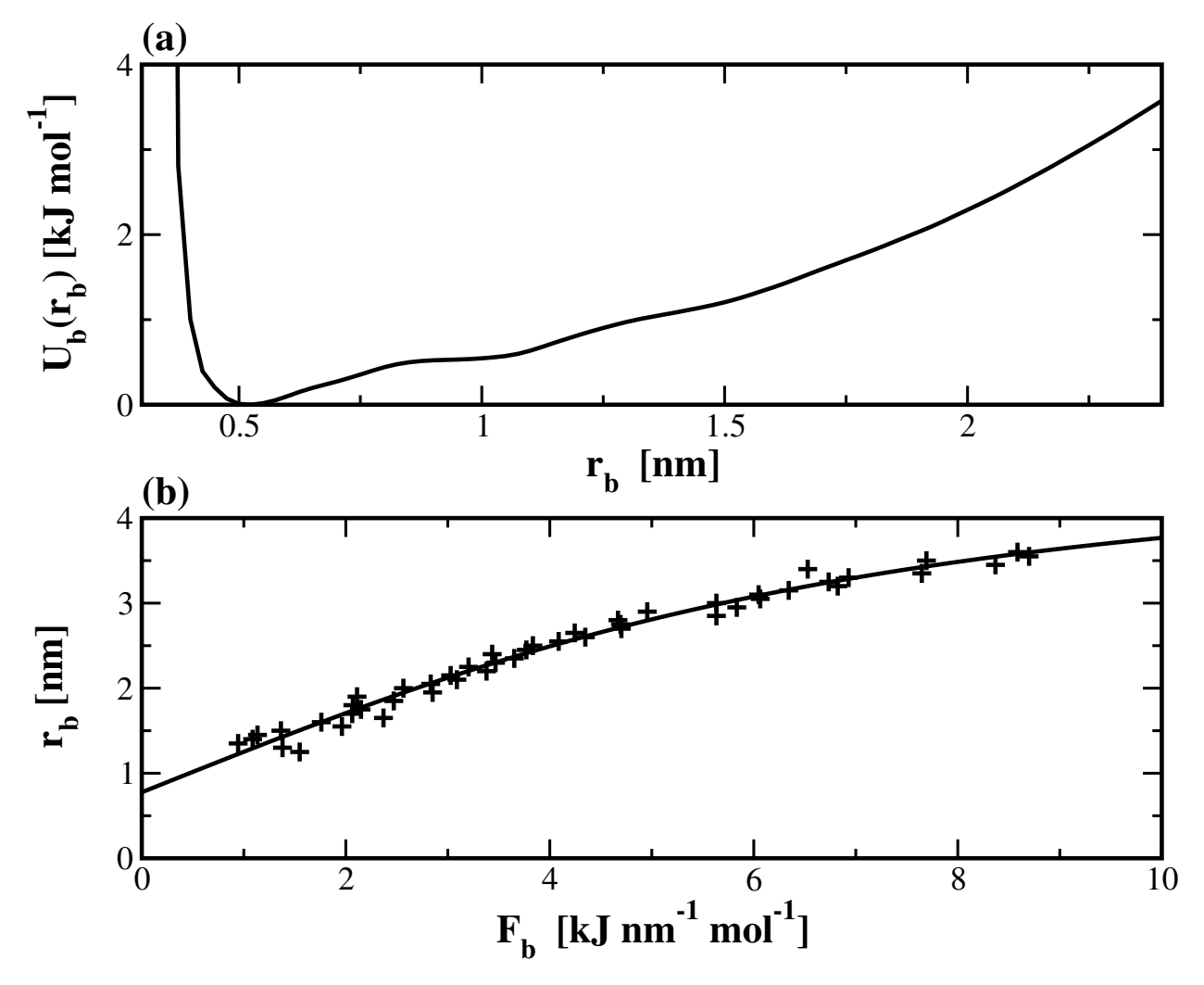


Figure 9: Panel (a) presents the calculated transferable bond potential, $U_b(r_b)$. Panel (b) compares the corresponding tension $F_b = +dU_b/dr_b$ (crosses) with the shifted Langevin curve for the average length of a freely jointed chain under equivalent tension (solid curve).

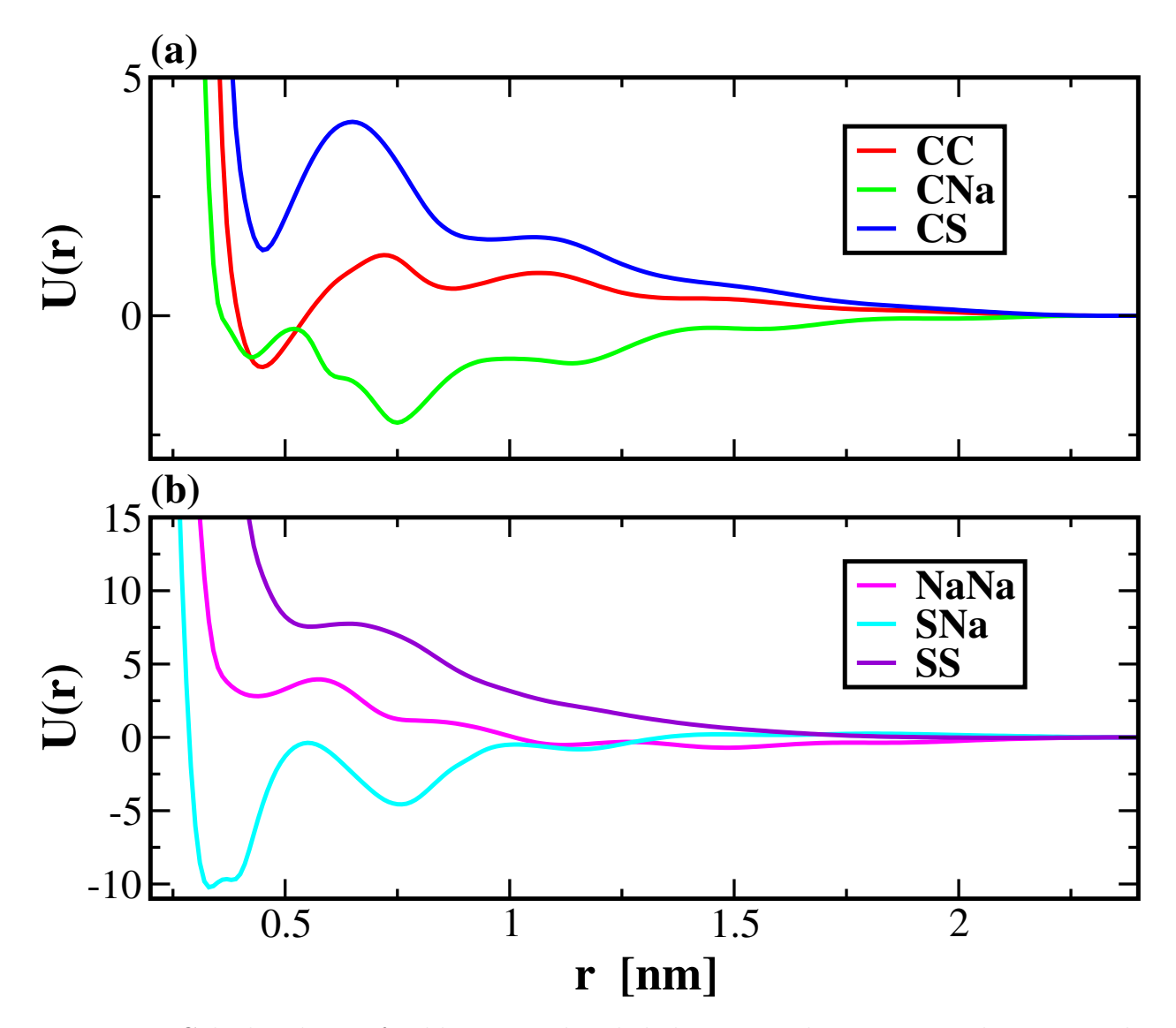


Figure 10: Calculated transferable xn non-bonded short-ranged pair potentials. Potentials are presented in units of $\rm kJ/mol$.

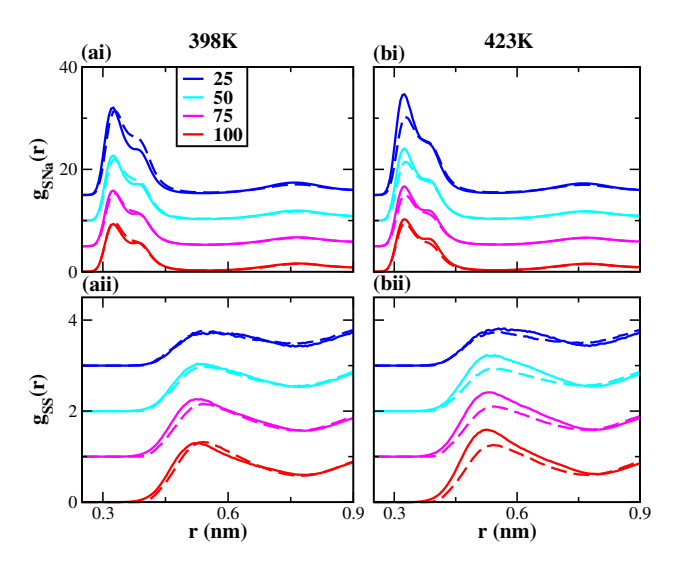


Figure 11: Comparison of simulated site-site rdfs in in the UA (solid curves) and in the initial transferable xn (dashed curves) models. Rows (i) and (ii) present the S-Na and S-S rdfs, respectively. In these two rows, the columns (a) and (b) present results for $T=398\mathrm{K}$ and $423\mathrm{K}$, respectively. The blue, cyan, magenta, and red curves present results for ionomer melts with 25, 50, 75, and 100% sulfonation, respectively

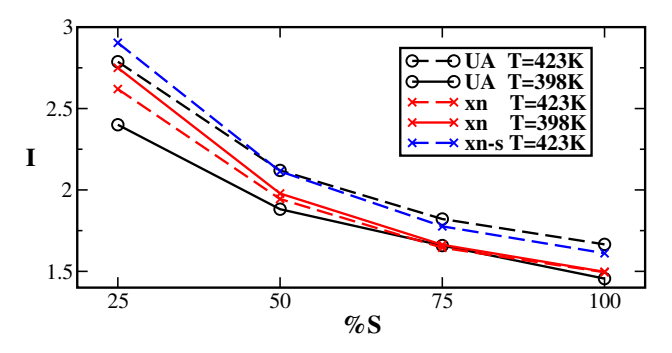


Figure 12: Equilibrium constant for charge aggregation as quantified by the area of the first peak in the S-Na rdf, $I = \int dr \, 4\pi r^2 g_{S-Na}(r)$ as a function of sulfonation, %S. The black and red curves correspond to the UA and to the initial xn models, respectively, while the solid and dashed curves correspond to $T=398 {\rm K}$ and 423K, respectively. The dashed blue curve presents results for the final xn model at $T=423 {\rm K}$ after heuristically rescaling the dielectric at this temperature.

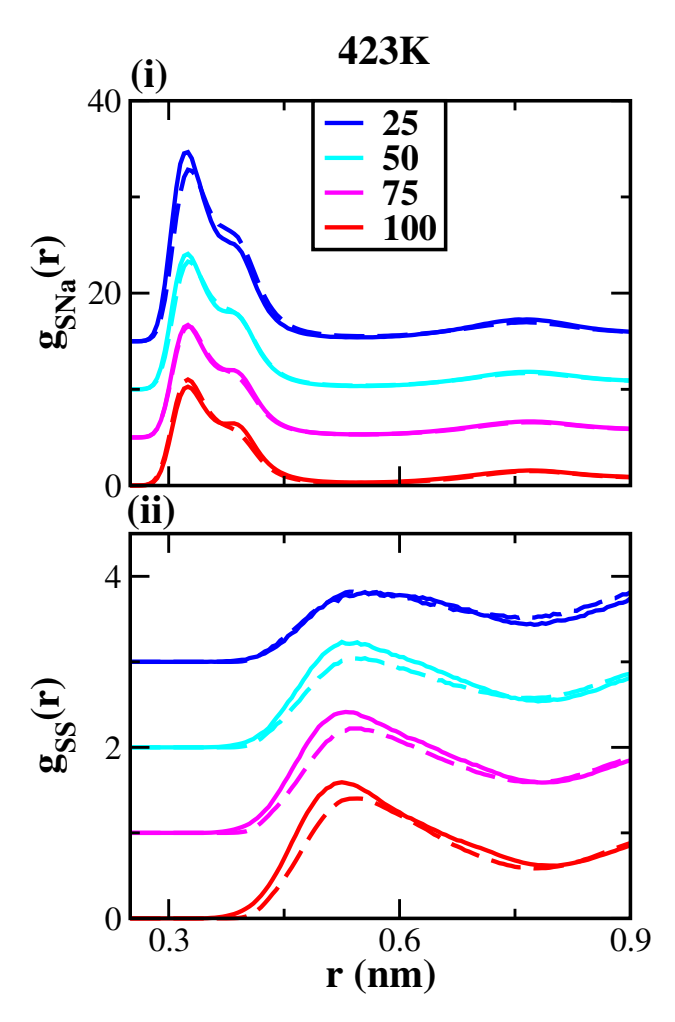


Figure 13: Comparison of simulated site-site rdfs at $T=423\mathrm{K}$ in the UA model (solid curves) and in the final transferable xn model (dashed curves) after rescaling the system-specific dielectrics at $T=423\mathrm{K}$. Rows (i) and (ii) present simulated rdfs for the S-Na and S-S site pairs, respectively. The blue, cyan, magenta, and red curves present results for ionomer melts with 25, 50, 75, and 100% sulfonation, respectively.

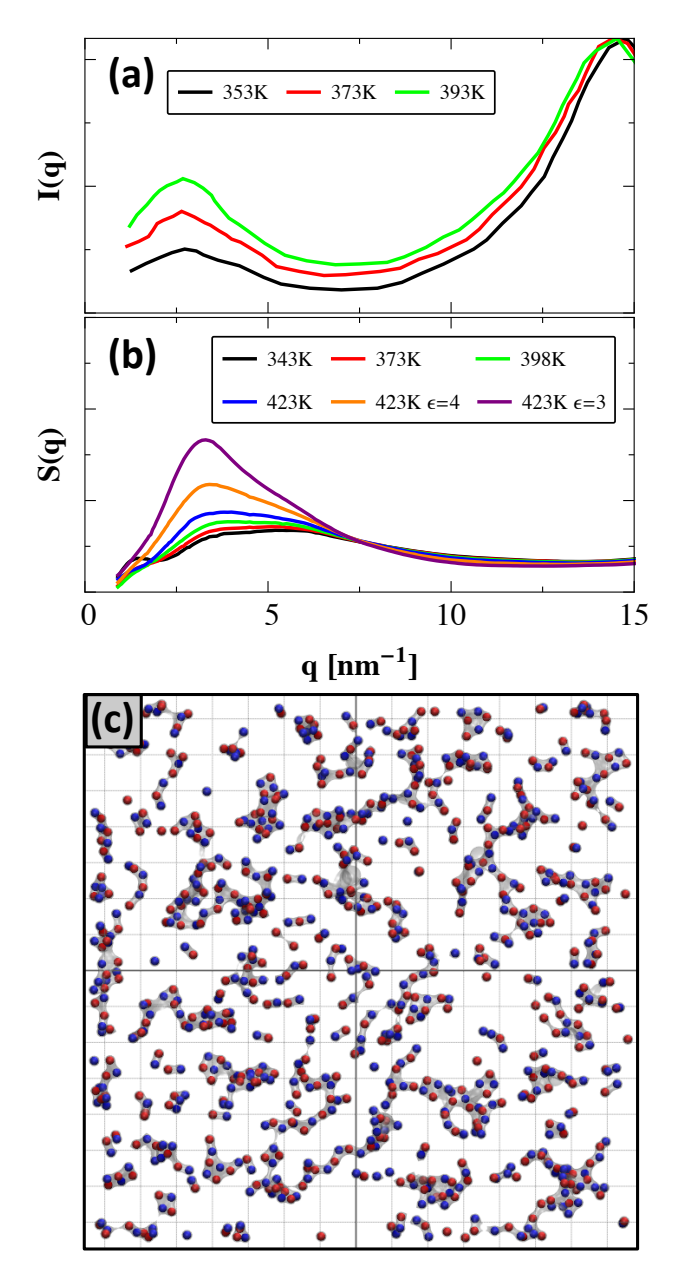


Figure 14: Comparison of experiments and simulations characterizing the temperature dependence of charge aggregation in the fully sulfonated ionomer melt. Panel (a) presents the ionomer feature in the measured X-ray scattering data extracted from Figure 1 of Ref. 69 after rescaling with respect to the "amorphous halo" feature at $q \approx 15 \text{ nm}^{-1}$. Panel (b) presents the structure factor calculated from simulations of the fully sulfonated ionomer with the xn-s force field. The orange and purple curves in panel (b) are calculated from CG simulations at 423K in which the dielectric constant has been further reduced to the values denoted in the legend. The bottom panel indicates the aggregation of cations (blue) and anions (red) in a simulated configuration of the fully sulfonated ionomer melt with the xn model at T=423 K after further reducing the dielectric to $\epsilon=3$. The image indicates the ions within a 2 nm slice through a cubic simulation box with sides of length L=15 nm, while the background provides a grid with 1 nm resolution in the x- and y- directions.

Graphical TOC Entry

